THE ELASTIC PROPERTIES OF FINE-GRAINED POLYCRYSTALLINE AND AMORPHOUS SAMPLES BY BRILLOUIN SCATTERING

BY

GUIMIAO ZHANG

THESIS

Submitted in partial fulfillment of the requirements
for the degree of Master of Science in Geology
in the Graduate College of the
University of Illinois at Urbana-Champaign, 2013

Urbana, Illinois

Adviser:

Professor Jay D. Bass

ABSTRACT

Near-perfect single crystals are often used for elasticity measurements when available, though in nature, fine-grained polycrystalline and amorphous minerals compose a large part of it. Therefore, the relationship between the properties of single-crystal and polycrystalline and amorphous samples is of fundamental importance in applying lab measurement results to real Earth. In this study we have investigated the sound velocities and elastic properties of fine-grained polycrystalline and amorphous materials using Brillouin scattering.

Our initial experiments were performed on silica minerals, among the most abundant minerals in the crust, and MgO, one of the major components of Earth's lower mantle. Four silica minerals (wood opal, hyalite, opal-CT and agate) and three MgO samples have been measured. The grain size of the silica minerals is around 1 to 7 micron in average, whereas that of the MgO is around 1 to 10 microns. Samples were ground and polished into plate-like shapes (~30 microns thick) for 90 ° geometry symmetric Brillouin scattering at room conditions, and for 50 ° geometry Brillouin scattering at high-pressure conditions. Our initial results at room conditions indicate that the velocities of agate, hyalite and wood opal are nearly 9%, 10% and 20% lower than the velocities obtained from single-crystal quartz measurements using Voigt-Reuss-Hill averaging respectively. Several features, such as the grain size, the inclusions and the water content, may

contribute to the velocities drops. However, Brillouin spectra from MgO samples up to 19GPa show broad peaks that are roughly symmetric in shape. Peak shifts and velocities of the fine-grained MgO are close to the velocities obtained from single-crystal MgO measurements. The sharpness of the peaks increases with the decreasing grain size. Some of our observations may be a result of grain boundary effects.

ACKNOWLEDGEMENTS

First of all, I have to express the depth of my gratitude to Professor Jay D. Bass, for his supervision on professional studies and suggestions on the life philosophy.

Second, I deeply appreciate Professor Lijun Liu, for his help with my thesis preparation and constructive advice on my future plan.

What is more, I sincerely thank all my previous and current labmates, namely Jia Chen, Armando Hermosillo, Seiji Kamada, Liqin Sang, and Jin Zhang, for helping me with the experimental procedures and getting integrated into American cultures.

In addition, I gratefully acknowledge Dr. G. Harlow (American Museum of Natural History, NY) for proving the opal samples, Dr. F. Bejina and Dr. M. Bystricky (Institut de Recherche en Astrophysique et Planétologie Observatoire Midi-Pyrénées, France) for proving the MgO synthetic samples, and S.K. Butler (ISGS) for the XRD analysis of the agate.

Finally, I would like to express my deep love to my family. Grew up with my grandparents, I learned all the basic living skills from them. Supported by my parents, I finished my college study. Encouraged by my fiancé, I went through the most depressed time. I believe, my life will go towards the sunshine with all my love companies.

Table of Contents

Chapter 1 Elastic properties of the natural earth

Abstract

The crust and mantle of the Earth are polycrystalline in nature, whereas in the laboratory we often measure properties on near-perfect single crystals when available. The relationship between the properties of single-crystal and polycrystalline samples is therefore of fundamental importance in applying laboratory measurements to the Earth. In addition, the relationship of grain size to elastic properties is important for controlling the properties of materials for industrial purposes.

Oxygen and silicon are the two most abundant elements in the earth's crust. Thus, it is not surprised that silica minerals are the most abundant oxides on the earth's surface. Nevertheless, research into the silica systems is motivated foremost by the prevalence of silica in man's immediate environment, and our knowledge of the silica mineral system has been through a huge expansion. However, the properties of microcrystalline and/or polycrystalline and even amorphous silica minerals remain highly uncertain.

The main components of the Earth's lower mantle are pervoskite (primarily $MgSiO_3$) and magnesiow üstite ((Mg,Fe)O). MgO, the magnesium (Mg) end member of (Mg,Fe)O solid solution, has a very broad stability field (atmospheric pressure to well beyond 100 GPa). Therefore the properties of magnesiowustite are of fundamental importance for understanding the Earth's lower mantle mineralogy. Although single-crystal MgO has

been extensively studied by experimental and theoretical methods, nano-crystalline MgO remains poorly understood.

1.1 Elastic properties measurements on the earth material

Since the early part of the 20th century, elastic modulus measurements have been recognized as essential for understanding the composition and structure of the Earth, especially deep portions of the Earth that are not sampled directly. This connection between elasticity and the properties of the deep Earth arises naturally, because the field of seismology provides us the acoustic wave velocities throughout the Earth, with ever increasing detail, whereas the acoustic velocities of minerals are in turn determined by their elastic moduli (Lay and Wallace, 1995). Williamson and Adams (1923) established a density and pressure distribution in the Earth by a few elastic wave velocity measurements on some rocks and bulk modulus measurements on iron. More recently, Tateno et al. (2010) explained the inner core seismic anisotropy on the basis of the elastic anisotropy of iron. The long-standing interest in experiments determination of the elastic properties of Earth materials only increase with time.

1.2 Silica minerals system

Oxygen and silicon are the two most abundant elements in the earth's crust, together constituting over 74 weight percentages of crustal rocks (Mason and Moore, 1982). The common occurrence of silica in sedimentary, igneous and metamorphic rocks has aroused

scientists' interests in silica as an indicator of geological processes, ranging from plate tectonics to the meteorites impacts (Heaney at al., 1994).

As one of the most common oxides in the crustal earth, silica or SiO_2 has distinct crystalline and microcrystalline forms in addition to amorphous forms (Table 1.1). Over the past decades, the properties and structures of single-crystal silica have been extensively studied. Scientists have constructed phase diagrams for the common silica polymorphs and measured the elastic properties of various polymorphs (Klein and Dutrow, 2007). However, the microcrystalline and amorphous forms are still poorly understood. Several difficulties are involved in measurements of the elastic properties of these forms of silica. Microcrystalline and amorphous silica often trap inclusions during formation and tend to crack easily. Therefore different pieces of the same sample may have significant aggregate compositions and microstructural differences. It is hard to isolate the effects of inclusions and to differentiate them from grain boundary effects and grain size effects, both of which may contribute to the elastic properties. The water content in the amorphous silica is another factor that can contribute to observed bulk elastic properties.

1.3 The importance of MgO in the earth

MgO is a simple oxide with the cubic NaCl type structure (Figure 1.1). It is stable to pressures above 100 GPa (Vassiliou and Ahrens, 1981; Mehl et al., 1988; Duffy et al.,

1995; Speziale et al., 2001), and is widely believed to be the second most abundant component in the lower mantle (Figure 1.2). There has been extensive previous work on the elasticity of MgO, including static compression experiments (Duffy et al., 1995; Utsumi et al., 1998; Fei, 1999), acoustic resonance and ultrasonic interferometry studies (Jackson and Niesler, 1982; Sumino et al., 1983; Isaak et al., 1989; Chen et al., 1998), shock wave experiments (Vassiliou and Ahrens, 1981; Svendsen and Ahren, 1987; Duffy and Ahrens, 1995), calorimetric measurements (Robie et al., 1978; Watanabe, 1982), vibrational spectroscopy measurements (Chopelas and Nicol, 1982; Chopelas, 1996), and Brillouin scattering measurements (Sinogeikin and Bass, 1999; Zha et al., 2001, Speziale et al., 2001). The abundant experiments to date have improved the knowledge of the thermal and elastic properties of the MgO, and offered relevant constrains for the lower mantle properties.

Although the single-crystal properties of MgO have been studied over the past forty years, the properties of nanocrystalline and/or polycrystalline MgO remain highly uncertain. Several difficulties contribute to this uncertainty. First, fine-grained MgO quickly reacts with atmospheric water to form the hydroxide mineral brucite $Mg(OH)_2$. Therefore sample preparation of fine-grained MgO is problematic. It is extremely difficult to remove all the water that may reside in the tiny interstices between grains. The kinetics of transformation of MgO to $Mg(OH)_2$ are rapid. Second, the contrast in elastic

properties of brucite and periclase is large (Table 1.2; Bass, 1995; Xia et al., 1998; Sinogeikin and Bass, 2000; Jiang et al., 2006). Only a small amount of $Mg(OH)_2$ formed by the reaction will result in a profound velocity drop. Thirdly, grain boundaries may dominate the Brillouin scattering experimental results by refracting the light inside the sample. The similar scales of the sample grain and the grain boundary limit the accuracy of the results. Since the nature of the crust and mantle of the Earth are polycrystalline, we need to develop a proper method to synthesis and study the polycrystalline MgO samples to better understand the Earth.

1.4 Brillouin Scattering

"Over the past few decades, Brillouin scattering has been used to measure the sound velocities for a wide range of materials of geophysical interest [for its particular importance in phases that are stable only at high pressures]." (Bass et al., 2008)

Figure 1.3 indicates the basic Brillouin scattering experimental layout combined with a Diamond Anvil Cell (DAC). The sound wave velocity can be determined by measuring the Brillouin frequency shift. Brillouin scattering was first applied to small single crystals of geological importance by Weidner et al. (1975). This work has been followed up by high-pressure Brillouin studies, which have been performed using a DAC on a number of mantle minerals (Brody et al., 1981; Duffy et al., 1995; Sinogeikin and Bass, 1999). Resistance heating and CO_2 laser heating support high temperature experiments for

Brillouin scattering (Sinogeikin et al., 2004; Jackson et al., 2004). Taneto et al. (2010) have already achieved over 330 GPa and 5500 K in the DAC experiments corresponding to the solid inner core conditions.

Therefore, combined with more advanced sample preparation technique, Brillouin scattering may offer a very powerful approach to study the elastic properties of the polycrystalline and/or amorphous candidate crustal earth and the polycrystalline candidate mantle mineral, MgO, and to interpret the geophysical observations.

References

Bass, J.D. (1995) Elasticity of minerals, glasses, and melts, in *Mineral Physics & Crystallography: A Handbook of Physical Constants, AGU Ref. Shelf*, vol. 2, edited by T. J. Ahrens, pp. 45–63, AGU, Washington, D. C.

Bass, J. D., Sinogeikin, S. V. and Li, B. (2008) Elastic properties of mineral: A key for understanding the composition and temperature of Earth's interior. *Elements*, 4, 165-170.

Brody, E. M., Shimizu, H., Mao, H. K., Bell, P. M. and Bassett, W. A. (1981) Acoustic velocity and refractive index of fluid hydrogen and deuterium at high pressures. *Journal of Applied Physics*, 52, 3583 - 3585

Chen, G., Liebermann, R. C. and Weidner, D. J. (1998) Elasticity of single-crystal MgO to 8 Gigapascal and 1600 Kelvin. *Science*, 280, 1913-1916

Chopelas, A. (1996). The fluorescence sideband method for obtaining acoustic velocities at high compressions: application to MgO and $MgAl_2O_4$. *Physics and Chemistry of Minerals*, 23, 25-37.

Chopelas, A., and M. Nicol (1982), Pressure Dependence to 100 Kilobars of the Phonons of MgO at 90 and 295 K. *Journal of Geophysical Research*, 87(B10), 8591–8597

Duffy, T. S. and Ahrens, T. J. (1995). Compressional sound velocity equation of state and constitutive response of shock-compressed magnesium oxide. *Journal of Geophysical Research,* 100, 529–542.

Duffy, T. S., Hemley, R. J. and Mao, H.-K. (1995) Equation of state and shear strength at multimegabar pressures: magnesium oxide to 227 GPa. *Physics Review Letter*, 74, 1371-1374.

Fei, Y. (1999) Effects of temperature and composition on the bulk modulus of (Mg,Fe)O. *American Mineralogist*, 84, 272–276.

Graetsch, H. (1994) Structural characteristics of opaline and microcrystalline silica mineral. *Review in mineralogy*, 29, 209-232.

Heaney, P. J., Prewitt, C. T. and Gibbs, G. V. (1994) Silica: Physical behavior, geochemistry and materials applications, pp iii-v. *Review in mineralogy*, vol 29

Hill, R. (1952) The elastic behavior of a crystalline aggregates. *Proceedings of the Physical Society Section A*, 65, 349–354.

Isaak, D. G., Anderson, O. L. and Goto, T. (1989) Measured elastic moduli of single-crystal MgO. *Physical Chemical Minerals*, 16, 704-713.

Jackon, I. And Niesler, H. (1982). The elasticity of periclase to 3 GPa and some Geophysical Implications. *Advances in the Earth and Plantetary Sciences*, 12, 93-113.

Jiang, F., Speziale, S. and Duffy, T.S. (2006) Single-crystal elasticity of brucite, $Mg(OH)_2$, to 15 GPa by Brillouin scattering. *American Mineralogist*, 91, 1893-1900.

Klein, C. and Dutrow, B. (2007) The 23rd Edition of The Manual of Mineral Science, pp524, Johns Wiley & Sons, Inc.

Lay, T. and Wallace, T.C. (1995) Modern Global Seismology. *Intemational geophysics series*, 58, Chapter 2, by Academic Press, Harcourt Place, 32 Jamestown Road, London NWl 7BY, UK.

Mason, B. and Moore, C. B. (1982) Principles of Geochemistry, 4th edn. John Wiley. New York

Mehl, M. J., Cohen, R. E. and Krakauer, H. (1988) Linearized plane wave electronic structure calculations for MgO and CaO. *Journal of Geophysical Research*, 93, 8009-8022.

Ono, S. (2008) Experimental Constraints on the Temperature Profile in the Lower Mantle, *Phys. Earth Planet. Inter.*, 170, 267–273.

Robie, R.A.; Hemingway, B.S.; Fisher, J.R. (1978) Thermodynamic properties of minerals and related substances at 298. 15 K and 1 bar pressure and at higher temperatures. *USGS-BULL*, 1452.

Sinogeikin, S. V. and Bass, J. D. (1999) Single-crystal elasticity of MgO at high pressure. *Physical Review B*, 59, R14141–R14144

Sinogeikin, S.V. and Bass, J.D. (2000) Single-Crystal Elasticity of Pyrope and MgO to 20 GPa by Brillouin Scattering in the Diamond Cell. *Physics of the Earth and Planetary Interiors*, 120(1–2), 43-62.

Sinogeikin, S. V., Lakshtanov, D. L., Nicolas, J. and Bass, J. D. (2004) Sound velocity measurements on laser-heated MgO and Al_2O_3. *Physics of the Earth and Planetary Interiors* 143-144, 575-586

Speziale, S., Zha, C.-S., Duffy, T. S., Hemley, R. J. and Mao, H. K. (2001) Quasi-hydrostatic compression of magnesium oxide to 52 GPa- Implications for the pressure-volume-temperature equation of state. *Journal of Geophysical Research*, 106, 515-528.

Sumino, Y., Anderson, O. L. and Suzuki, I. (1983) Temperature coefficients elastic constrains of single crystal MgO between 20 and 1300 K. *Physical Chemical Minerals*, 9, 38-47.

Svendsen, B. and Ahrens, T. J. (1987) Shock-induced temperatures of MgO. *Geophysical Journal of the Royal Astronomical Society*, 91, 667–691.

Tateno, S., Hirose, K., Ohishi, Y. and Tatsumi, Y. (2010). The structure of iron in Earth's Inner Core. *Science*, 330, 359-361.

Utsumi, W., Weidner, D. J. and Liebermann, R. C. (1998) Volume measurement of MgO at high pressures and high temperatures, in *Properties of earth and planetary materials at high pressure and temperature*, edited by M. H. Manghnani and T. Yagi, Geophysical Monograph 101, American Geophysical Union, 217-333.

Vassiliou, M. S. and Ahrens, T. J. (1981) Hugoniot equation of state of periclase to 200 GPa. *Geophysics Research Letter*, 8, 729

Weidner, D. J., Swyler, K. and Carleton, H. R. (1975) Elasticity of microcrystals. *Geophyical Research Letters*, 2, 189-192.

Xia, X., Weidner, D.J. and Zhao, H. (1998) Equation of state of brucite; single-crystal Brillouin spectroscopy study and polycrystalline pressure-volume-temperature measurement. *American Mineralogist*, 83(1-2), 68-74.

Zha, C.-S., Mao, H.-K. and Hemley, R.J. (2000) Elasticity of MgO and a primary pressure scale to 55 GPa. *PNAS*, 97, 13494–13499

Tables

Table 1.1 Polymorphs of SiO_2, after Grartsch (1994)

	phase	crystal symmetry / variety
Crystalline	α-quartz	trigonal
	β-quartz	hexagonal
	α-tridymite	orthorhombic
	β-tridymite	hexagonal
	α-cristobalite	tetragonal
	β-cristobalite	cubic
	coesite	monoclinic
	stishovite	tetragonal
	moganite	monoclinic
Microcrystalline	agate	intergrowth of quartz and moganite
	opal-C	disordered cristobalite
	opal-CT	disordered cristobalite and tridymite
Amorphous	opal-A	Also known as hylite

Table 1.2 Acoustic wave velocities of MgO and $Mg(OH)_2$ at ambient temperature and pressure

VRH average	MgO	$Mg(OH)_2$
Vs (m/s)	6032	3846
Vp (m/s)	9697	6154

1. VRH average: Voigt-Reuss-Hill average velocities calculated using the Hill averaging scheme (Hill, 1952).
2. Velocities for MgO used data from Sinogeikin and Bass (2000).
3. Velocities for $Mg(OH)_2$ used data from Jiang et al. (2006).

Figures

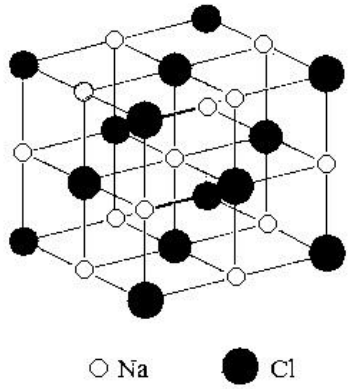

Figure 1.1. NaCl structure. In MgO, Mg substitutes for Na, while O substitutes for Cl. The ionic radius of O will be larger than Mg. MgO is the elastically anisotropic due to its crystal structure.

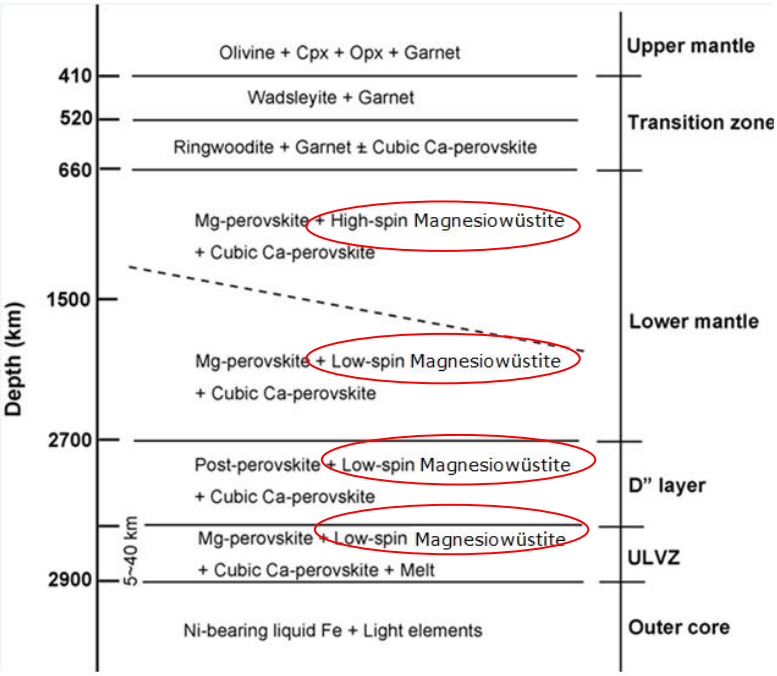

Figure 1.2. Mineral compositions from upper mantle to outer core. (Mg, Fe)O is one of the major components from 660km to 2900km (lower mantle). (Modified after Ono, 2008)

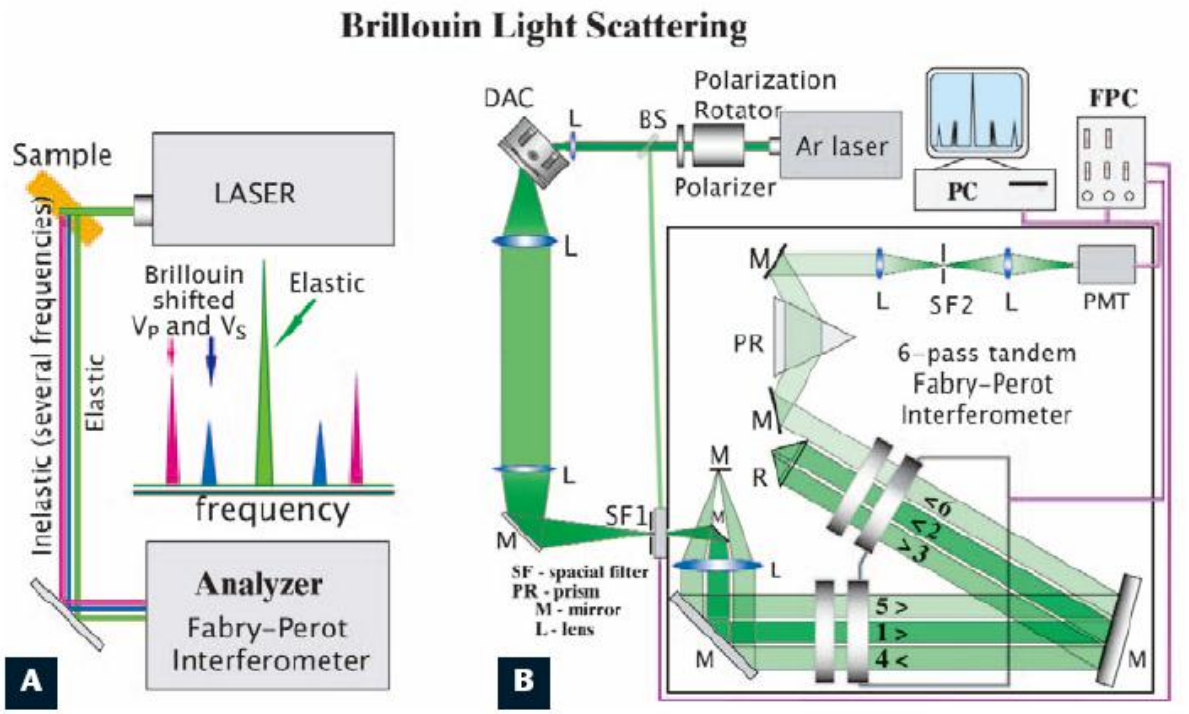

Figure 1.3. (A) General schematic for most light-scattering experiments. Laser light hits the sample and the scattered light is analyzed. (B) A more complete diagram of a Brillouin-scattering experiment using a sample at high pressure in a DAC. PC = personal computer; PMT =photomultiplier tube; FPC = Fabry-Perot controller; BS = beam splitter. (Bass et al., 2008) During ambient condition measurements, a sample in the air will substitute for the DAC.

Chapter 2 Silica minerals elastic properties measurements at ambient conditions

Abstract

Amorphous and polycrystalline forms of silica minerals trap inclusions during formation and tend to crack easily. Opal and agate are two common amorphous and polycrystalline forms of silica. The water component constitutes a substantial fraction of the weight. The effective elastic behaviors of water content, grain size and inclusions are still poorly understood. Here, acoustic aggregate compressional and shear wave velocities of opal and agate were measured by Brillouin scattering at ambient condition. The major reasons for different samples velocities drops were discussed.

2.1 Introduction

Amorphous and polycrystalline forms of silica minerals may have different grain size, ranging from a few nanometers to tens of microns. Opal, which can contain 3% to 21% weight percent total water content, is one of the most commercially important amorphous and polycrystalline forms of silica minerals (Graetsch, 1994; Langer and Flörke, 1974), as well as agate.

During the past century, several studies have been done to understand the α-β quartz phase transition: thermodynamic properties and elastic constant variations (Carpenter, 1998); grain size effect (Ríos et al, 2001); and the influence of water content (Ito and

Nakashima, 2002). However, the variations of elasticity, specifically sound velocities, due to the grain size, water content and the presence of inclusions are still poorly understood.

2.2 Experimental details

Four natural samples were involved in this Brillouin spectroscopy study. Details of the sample description are shown in table 2.1. Samples were ground and polished into plate-like shapes for platelet-symmetric geometry Brillouin scattering at room conditions. An Ar laser (λ = 514.5 nm) was used as a light source, and the scattered light was analyzed with a 6-pass piezoelectrically scanned Fabry-Perot interferometer. A Scintag XDS2000 powder diffractometer was used X-ray diffraction measurements on agate to identify crystalline compounds by matching diffraction patterns to a database.

2.2.1 Brilloun scattering

Brillouin scattering, named after Léon Brillouin, is the inelastic scattering of visible light that occurs when incident light in a medium (such as air, water or a crystal) interacts with time-dependent optical density variations, resulting in a change in its energy (frequency) and direction (Brillouin, 1922, 1930). From a quantum perspective, Brillouin scattering is an interaction between an electromagnetic wave and a density wave (photon-phonon scattering), magnetic spin wave (photon-magnon scattering), or other low frequency quasiparticle, resulting in an energy change (Sandercock, 1982; Bass, 2007). The photon may lose energy to create a quasiparticle (Stokes process) or gain

energy by destroying one (anti-Stokes process), which influences the scattered photon frequency. The shift in photon frequency, known as the Brillouin shift, is equal to the energy of the interacting phonon or magnon and thus Brillouin scattering can be used to measure phonon or magnon energies:

$$v = \frac{c(\omega_i - \omega_s)}{\omega_i (n_i^2 + n_s^2 - 2n_i n_s \cos\theta)^{1/2}},$$

where ν is the velocity of the acoustic wave; c is the light speed; n is the refractive index; ω is the frequency; and θ is the scattering angle between the incident (i) and scattered (s) wave vectors (Figure 2.1; Angle et al., 2009). In our experiments, the samples are polycrystalline and amorphous forms. If there is no preferred orientation inside the polycrystals, in another word, the samples are isotropic, the expression above will simplify as

$$v = \frac{\Delta\omega \cdot \lambda}{2\sin(\theta^*/2)}$$

where θ^* is the external angle between the incoming and scattered light directions outside the sample (Figure 2.2; Whitfield et al., 1976; Sinogeikin and Bass, 2000; Bass, 2007).

The Brillouin shift is commonly measured by the use of a Brillouin spectrometer, the key component of which is a Fabry–Pérot (FP) interferometer. The intensities of the Brillouin shifted components of the scattered light are very small (usually at least an order of magnitude less than the Rayleigh scattered light) , with frequency shifts typically

in the range of tens of GHz. A FP interferometer is well-suited to resolve those frequency shifts (Figure 1.3B). The intrinsic precision of Brillouin spectroscopy is within one to five out of a thousand (Sandercock, 1982; Angle et al., 2009).

2.2.2 X-ray powder diffraction

X-ray, discovered by Max von Laue in 1912, has a similar wavelength range to the spacing of planes in a crystal lattice (Warren, 1969). X-ray diffraction is now a common technique for the study of crystal structures and atomic spacing (Klug and Alexander, 1974; Cosier and Glazer, 1986; Heying et al., 1996; Rose-Petruck et al., 1999; Siders et al., 1999).

X-ray diffraction is based on constructive interference of monochromatic X-rays and a crystalline sample (Chatterjee, 2008; Als-Nielsen and McMorrow, 2011). The interaction of the incident rays with the sample produces constructive interference (and a diffracted ray) when conditions satisfy Bragg's Law,

$$n\lambda = 2d\sin\theta,$$

(Figure 2.3; Chatterjee, 2008), which relates the wavelength of electromagnetic radiation to the diffraction angle and the lattice spacing in a crystalline sample. All possible diffraction directions of the lattice should be attained due to the random orientation of the powdered material by scanning the sample through a range of 2θ angles. Since each mineral has a set of unique d-spacings, mineral identification can be achieved by

comparison of d-spacings with standard reference patterns (Warren, 1969; Connolly, 2007; Chatterjee, 2008; Als-Nielsen and McMorrow, 2011).

2.2.3 Water content measurements

Samples were meshed into small pieces and put into a ceramic/platinum container. Samples were heated up to 1000 ℃ for 24 hours using Barnstead Thermolyne 1300 furnace. The weight of the sample was measured both before and after heating using Metler Toledo AL104 electronic balance. The water content was calculated as the difference of the weight.

2.3 Results and discussions

Opal#C81366 (hyalite) is clear with a grain size less than one micron. Under the petrographic microscope, we cannot observe any inclusions within the sample. Brillouin spectra were collected over an angular range of 180 ºspaced 30 ºapart in the sample plane at ambient condition (Table 2.2). The Brillouin peaks were generally of very good quality with a high signal-to-noise ratio and symmetrically sharp peaks (Figure 2.4). Probing different orientations of this sample yield roughly the same velocities, which is also consistent with the homogeneous appearance of the sample. The standard deviation of the acoustic wave velocities is within one percent.

Opal#C81438 (wood opal) is classified as wood opal. Since this sample has a clear striped interlocking structure, two parts (light yellow part and dark brown part) of the

sample were analyzed by the Brillouin spectroscopy. Brillouin spectra were obtained over an angular range of 180 ºspaced 30 º(dark brown part; 15 º, light yellow part) apart in the sample plane at ambient condition (Table 2.3). The Brillouin peaks were roughly symmetric in shape with a low signal-to-noise ratio (Figure 2.5). The presence of aligned inclusions likely contributes to the high noise background. The standard deviation of the acoustic wave velocities is within two percent. The difference between dark part velocities and light part velocities is around 1%. Hence, for this particular wood opal, the color of the sample does not appear to significantly influence the acoustic wave velocities.

Opal#C81482 (opal-CT) is translucent even with 15μm thickness, and therefore Brillouin spectra cannot be collected. Opal-CT has been interpreted as consisting of clusters of stacking of cristobalite and tridymite over very short length scales. The spheres of opal in opal-CT are themselves made up of tiny microcrystalline blades of cristobalite and tridymite (Graetsch, 1994). Therefore this special microcrystalline structure leads to the difficulty to obtain Brillouin spectra.

Brillouin spectra for agate were obtained over an angular range of 180 ºspaced 30 º apart in the sample plane at ambient condition (Table 2.4). The Brillouin peaks were generally of good quality with a relatively high signal-to-noise ratio and symmetrically broad peaks (Figure 2.6). At some specific chi angels, there are more than two peaks. One

possibility of the extra peaks is that they are peaks of moganite, because agate is very fine intergrowths of the minerals quartz and moganite (Graetsch, 1994). X-ray powder diffraction was performed to determine the existence of moganite. The result indicates that there is only quartz in this agate sample (Figure 2.7). The other possibility is that Brillouin probe was sensing two different orientation quartz grains, which requires those peaks falling into the anisotropy zone of quartz. Previous studies on single-crystal quartz suggest that quartz is highly anisotropic elastically with values of $\Delta Vp/Vp^{*}$ = 17.1%, $\Delta Vs/Vs^{*}$ = 26.9%, where ΔVp and ΔVs are the differences between the maximum and minimum velocities for the crystal longitudinal and shear, respectively; and Vp^{*} (6048m/s) and Vs^{*} (4090m/s) are aggregate velocities calculated using the Hill averaging scheme (Hill, 1952; Schulz et al., 1970; Bass, 1995). Thus, the extra peaks are due to the attached two grains.

Table 2.5 shows the summary of silica minerals Brillouin measurements. The velocities of agate, hyalite and wood opal are nearly 9%, 10% and 20% lower than the velocities obtained from single-crystal quartz measurements using Voigt-Reuss-Hill averaging respectively. The velocities contrasts between our samples and the silica glass (Zha et al., 1994; Zhang et al, 2011) are smaller. There are several reasons contributing to the velocities contrasts, such as the water content, the inclusions and the grain boundaries.

Hyalite, amorphous form of silica, is homogeneous in nature. It contains more than 10% water (Graetsch, 1994). Thus, the only reason for its velocity drop is the water content. The certain relationship between water content and velocity drop can be established if experiments can be conducted on different water content hyalite samples.

Wood opal is a form of petrified wood which has developed on opalescent sheen (Graetsch, 1994). Thus, wood opal traps inclusions during formation and tends to crack easily. Compared to the small grain size (under one micron), the abundant inclusions occupy large volume of the sample, resulting in noisy spectra. The inclusions influence the velocities drops in addition to the water content effect.

Agate is relatively dry form of silica with around 7μm grain size. Thus, the water content is not the major reason of its velocities drops. There is a preferred orientation in a short distance range. Thus, we conclude the velocities drops are always due to the averaging of two different oriented grains and the grain boundaries.

Table 2.6 shows the preliminary results of the water content measurements. The acoustic wave velocities decrease as the increasing water content (figure 2.8), which confirm our hypothesis that the water content will contribute to the velocities drop. However, this is not the only reason for the velocities contrasts. The silica glass (Corning 7980) using as the reference has only an ignorable amount of water in it. Compared with agate, which has about 4% water, silica glass has lower velocities. Thus, we cannot

simply conclude that the higher the water content, the lower the acoustic velocities.

2.4 Conclusions

Several features, such as the inclusions, the water content and the grain boundaries, can influence the Brillouin spectra's quality and lead to decreased aggregate velocities. The velocities of different forms of silica can be decreased by a variety of factors.

References

Als-Nielsen, J., and McMorrow, D. *Elements of Modern X-ray Physics*. 2nd ed. Hoboken: Wiley, 2011.

Angel, R.J., Jackson, J.M., Reichmann, H.J. and Speziale, S. (2009) Elasticity measurements on minerals: a review. *European Journal of Mineralogy*, 21, 525-550.

Bass, J.D. (1995), Elastic properties of minerals, melts, and glasses, in: *Handbook of Physical Constants*, edited by T.J. Ahrens, American Geophysical Union special publication, pp. 45-63

Bass, J.D. (2007) Theory and Practice – Techniques for Measuring High P/T Elasticity. *Treatise on Geophysics*, 2, 269-291.

Brillouin, L. (1922) Théorie des quanta et l'atome de Bohr. *Recueil des conférences-rapports de documentation sur la physique*, 2(1). La Société, Paris.

Brillouin, L. (1930) Les électrons dans les métaux et le classement des ondes de de Broglie correspondantes. *Comptes Rendus Hebdomadaires des Séances de l'Académie des Sciences*, 192(292).

Carpenter, M.A., Salje, E.K., Graeme-Barber, A., Wruck, B., Dove, M.T. and Knight, K.S. (1998). Calibration of excess thermodynamic properties and elastic constant variations associated with the α-β phase transition in quartz. *American mineralogist*, 83(1), 2-22.

Chatterjee, A. K. (2008). X-ray diffraction. *Handbook of Analytical Techniques in Concrete Science and Technology: Principles, Techniques and Applications*, 275.

Connolly, J.R. (2007) Introduction to X-Ray Powder Diffraction. Can be retrieved: http://epswww.unm.edu/xrd/xrdclass/01-XRD-Intro.pdf

Cosier, J.T. and Glazer, A.M. (1986). A nitrogen-gas-stream cryostat for general X-ray diffraction studies. *Journal of applied crystallography*, 19(2), 105-107.

Graetsch, H. (1994) Structural characteristics of opaline and microcrystalline silica mineral. *Review in mineralogy*, 29, 209-232

Heying, B., Wu, X.H., Keller, S., Li, Y., Kapolnek, D., Keller, B.P., and Speck, J. S. (1996). Role of threading dislocation structure on the x-ray diffraction peak widths in epitaxial GaN films. *Applied physics letters*, 68(5), 643-645.

Ito, Y. and Nakashima, S. (2002). Water distribution in low-grade siliceous metamorphic rocks by micro-FTIR and its relation to grain size: a case from the Kanto Mountain region, Japan. Chemical geology, 189(1), 1-18.

Klug, H.P., and Alexander, L.E. (1974). X-ray diffraction procedures: for polycrystalline and amorphous materials. *X-Ray Diffraction Procedures: For Polycrystalline and Amorphous Materials, 2nd Edition, by Harold P. Klug, Leroy E. Alexander, pp. 992.*

Langer,K. and Flörke, O.W. (1974) Near infrared absorption spectra (4000–9000 cm^{-1}) of opals and the role of water in these $SiO_2 \cdot nH_2O$ minerals. *Fortschritte der Mineralogie*, 52, 17-51.

Ríos, S., Salje, E.K.H. and Redfern, S.A.T. (2001). Nanoquartz vs. macroquartz: a study of the α↔β phase transition. *The European Physical Journal B-Condensed Matter and Complex Systems*, 20(1), 75-83.

Rose-Petruck, C., Jimenez, R., Guo, T., Cavalleri, A., Siders, C.W., Rksi, F. and Barty, C.P. (1999). Picosecond–milliångström lattice dynamics measured by ultrafast X-ray diffraction. *Nature, 398*(6725), 310-312.

Sandercock, J.R. (1982) Trends in brillouin scattering: Studies of opaque materials, supported films, and central modes. In: *Topics in Applied Physics Volume 51: Light Scattering in Solids III*, pp 173-206. Berlin: Springer-Verlag.

Schulz, M.B., Matsinger, B.J. and Holland, M.G. (1970). Temperature dependence of surface acoustic wave velocity on α quartz. *Journal of Applied Physics*, 41(7), 2755-2765.

Siders, C.W., Cavalleri, A., Sokolowski-Tinten, K., Toth, C., Guo, T., Kammler, M., and Barty, C.P.J. (1999). Detection of nonthermal melting by ultrafast X-ray diffraction. *Science*, 286(5443), 1340-1342.

Sinogeikin, S.V., and Bass, J.D. (2000) Single-Crystal Elasticity of Pyrope and MgO to 20 GPa by Brillouin Scattering in the Diamond Cell. *Physics of the Earth and Planetary Interiors*, 120(1–2), 43-62.

Soga, N. (1968). Temperature and pressure derivatives of isotropic sound velocities of α quartz. Journal of Geophysical Research, 73(2), 827-829.

Warren, B. E. (1969). *X-ray Diffraction*. Courier Dover Publications.

Whitfield, C.H., Brody, E.M. and Bassett, W.A. (1976) Elastic moduli of NaCl by Brillouin scattering at high pressure in a diamond anvil cell. *Review of Scientific Instruments* 47, 942-947.

Zha, C.S., Hemley, R.J., Mao, H.K., Duffy, T.S. and Meade, C. (1994). Acoustic velocities and refractive index of SiO_2 glass to 57.5 GPa by Brillouin scattering.

Physical Review B, 50(18), 13105.

Zhang, J.S., Bass, J.D., Taniguchi, T., Goncharov, A.F., Chang, Y.Y. and Jacobsen, S.D. (2011). Elasticity of cubic boron nitride under ambient conditions. *Journal of Applied Physics*, 109, 063521.

Tables

Table 2.1 Silica Sample descriptions

Species	Sample #	Location	Note
Opal	C81366	San Luis Potosi, Mexico	Opal-A, also known as hyalite; transparent after preparation
Opal	C81438	Transylvania, Romania	Wood opal; transparent after preparation
Opal	C81482	Durango, Mexico	Opal-CT; translucent even with 15μm thickness
Agate	-	-	transparent after preparation

Table 2.2 Opal#C81366 Results of Brillouin spectral data.

Chi angle	Vs (m/s)	Vp (m/s)
180	3558	5629
210	3565	5634
240	3568	5629
270	3584	5662
300	3590	5685
330	3596	5687
360_01	3544	5601
360_02	3574	5653
360_03	3603	5694
360_04	3526	5563
360_05	3551	5612
average	3569 ± 23	5641 ± 40
±σ	0.66%	0.72%

1. 360_01 ~ 360_05 were collected to examine the range of velocity variations from probing different sample positions.
2. ±σ: One Standard Deviation of peak position

Table 2.3 Opal#C81438 Results of Brillouin spectral data

Chi angle	Light yellow part		Dark brown part	
	Vs (m/s)	Vp (m/s)	Vs (m/s)	Vp (m/s)
180	3101	4797	3111	4778
197	3125	4813		
210	3091	4785	3128	4740
225	3158	4792		
240	3132	4810	3114	4738
257	3106	4791		
270	3115	4770	3022	4820
285	3105	4784		
300	3130	4790	3022	4684
315	3102	4771		
330	3094	4856	3099	4695
345	3147	4830		
360	3093	4829	3103	4728
360			3104	4741
360			3091	4721
average	3115 ± 21	4801 ± 25	3088 ± 39	4738 ± 42
±σ	0.69%	0.52%	1.26%	0.88%

1. For dark part of opal#C81438, Brillouin spectra were collected at 360 chi angle three times. Different sample positions were probed at that specific chi angle.
2. ±σ: One standard deviation of peak position

Table 2.4 Agate results of Brillouin spectral data

Chi angle	V_1 (m/s)	V_1' (m/s)	V_2 (m/s)	V_2' (m/s)
360	5791		3724	
330	5795		3782	
300	5624		3903	3680
270	5843		3775	
240	5850		3767	
210	5665		3902	
180	5991	5472	4030	3669
average	5720 ±139		3804 ±119	
±σ	2.44%		3.13%	

1. ±σ: Standard Deviation of peak position.
2. When we calculated the average and ±σ for V_1, we consider V_1 and V_1' together. When we calculated the average and ±σ for V_2, we consider V_2 and V_2' together.

Table 2.5 Summary of silica minerals sound velocities

m/s	Vs	Vp	Velocity contrast with quartz		Velocity contrast with silica glass	
			S-wave	P-wave	S-wave	P-wave
hyalite	3569 ±23	5641 ±40	-12.7%	-6.7%	-5.0%	-4.5%
wood opal	3104 ±32	4775 ±45	-24.1%	-21.0%	-17.4%	-19.1%
agate	3804 ±119	5720 ±139	-7.0%	-5.4%	1.3%	-3.1%

1. Quartz acoustic wave (Vs = 4090 m/s, Vp = 6048 m/s) velocities are calculated using Voigt-Reuss-Hill averaging according to Bass, 1995.
2. Silica glass acoustic wave velocities (Vp = 5905.5±0.8 m/s, Vs = 3755.9±0.6 m/s) were obtained from ultrasonic studies (Zhang et al, 2011).

Table 2.6 Results of silica minerals water content measurements

mg	Before heating		After heating		water content
	C	C+S	C	C+S	
hyalite	55894.1(1)	55916.1(1)	55894.0(1)	55911.8(1)	19%
wood opal	5407.0(1)	5444.0(1)	5406.9(1)	5433.8(1)	27%
agate	5406.1(1)	5585.5(1)	5406.1(1)	5577.9(1)	4%

1. C: container
   S: sample.
2. Water content is calculated as the weight difference between before and after heating.

Figures

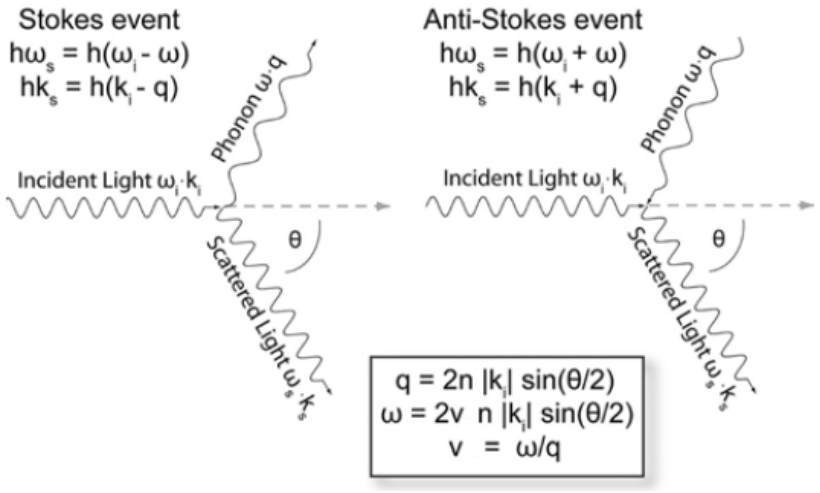

Figure 2.1 Schematic of the two types of inelastic interaction between incident radiation and the vibrational modes in a crystal, as represented by phonons. In a Stokes event the energy is transferred to the phonon, and the energy of the scattered radiation is reduced. In an anti-Stokes event, the energy is transferred from the phonon to the radiation, which is thus increased in energy. In the figure, h is Planck's constant; ω circular frequency, k photon wave vector, q phonon wave vector; θ scattering angle; n refractive index; v acoustic velocity. (Angel et al., 2009)

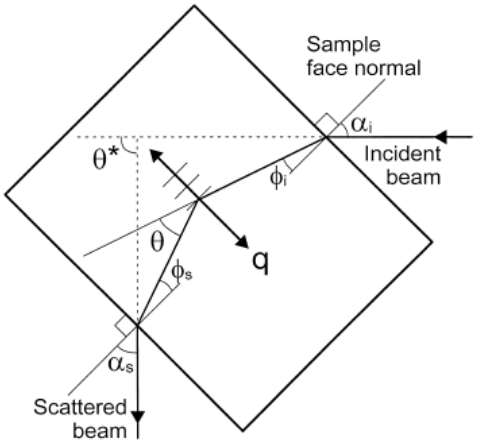

Figure 2.2 Platelet, or symmetric, scattering geometry. Solid lines indicate directions of the incident and scattered beams in the sample (rectangle). A and f are the angles between the incident (i) and scattered (s) beams and sample face normals. q is the phonon direction. θ is the actual scattering angle, and θ^* is the external scattering angle. (Sinogeikin and Bass, 2000).

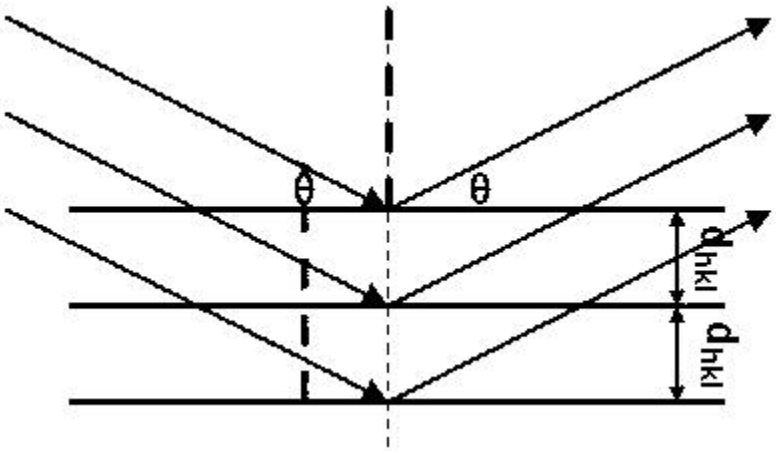

Figure 2.3 Schematic of X-ray diffraction obeying Bragg's Law**.**

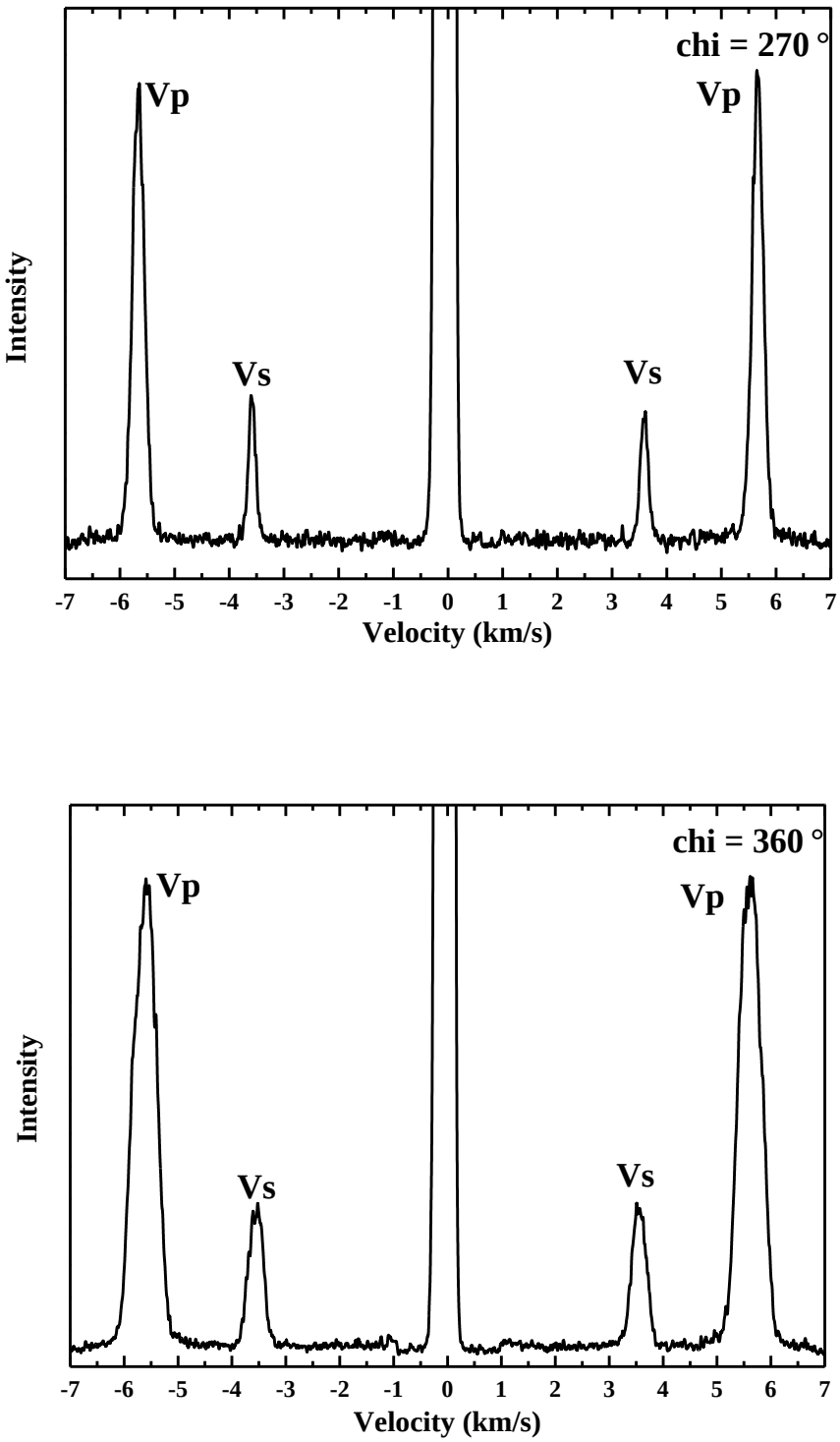

Figure 2.4 Two typical Brillouin spectra for opal#C81366 at different chi angles. The center peak is the Rayleigh peak. Compression and shear wave peaks are all roughly symmetric.

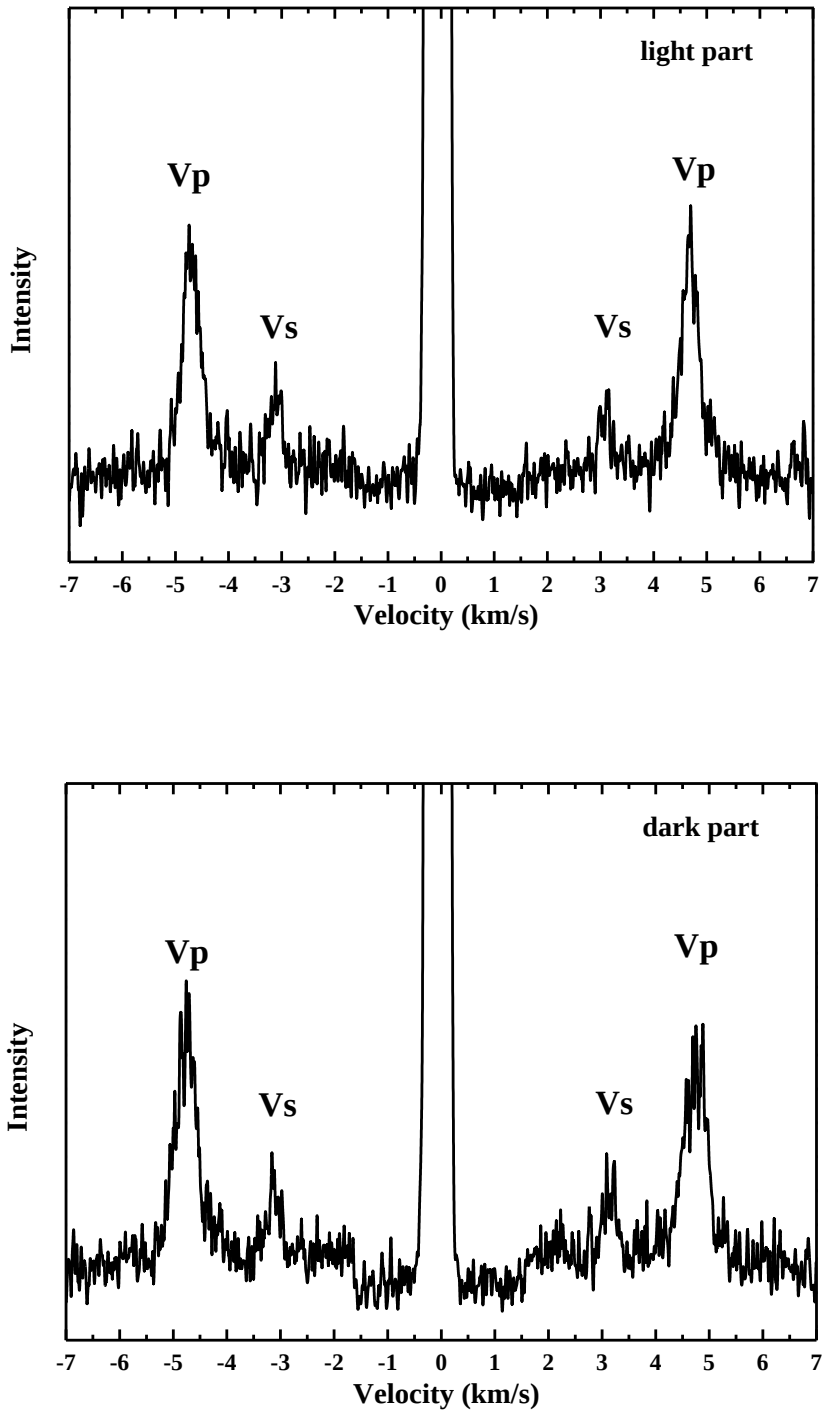

Figure 2.5 Two typical Brillouin spectra for opal#C81438 at same chi angles. The center peak is the Rayleigh peak. Compression and shear wave peaks are all roughly symmetric.

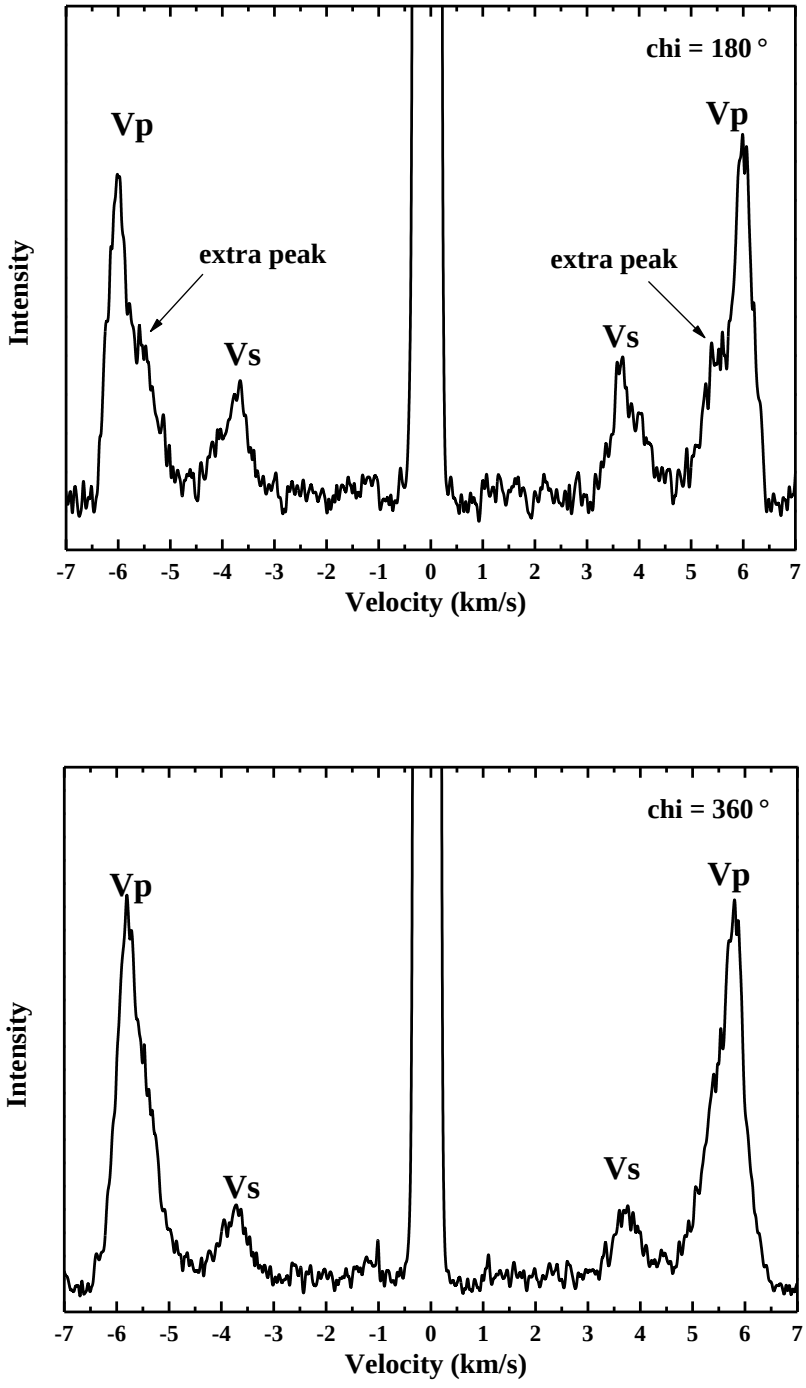

Figure 2.6 Two typical Brillouin spectra for agate at different chi angles. The center peak is the Rayleigh peak. Compression and shear wave peaks are all roughly symmetric. At some chi angles, there are more than one shear (compressional) wave peaks.

.

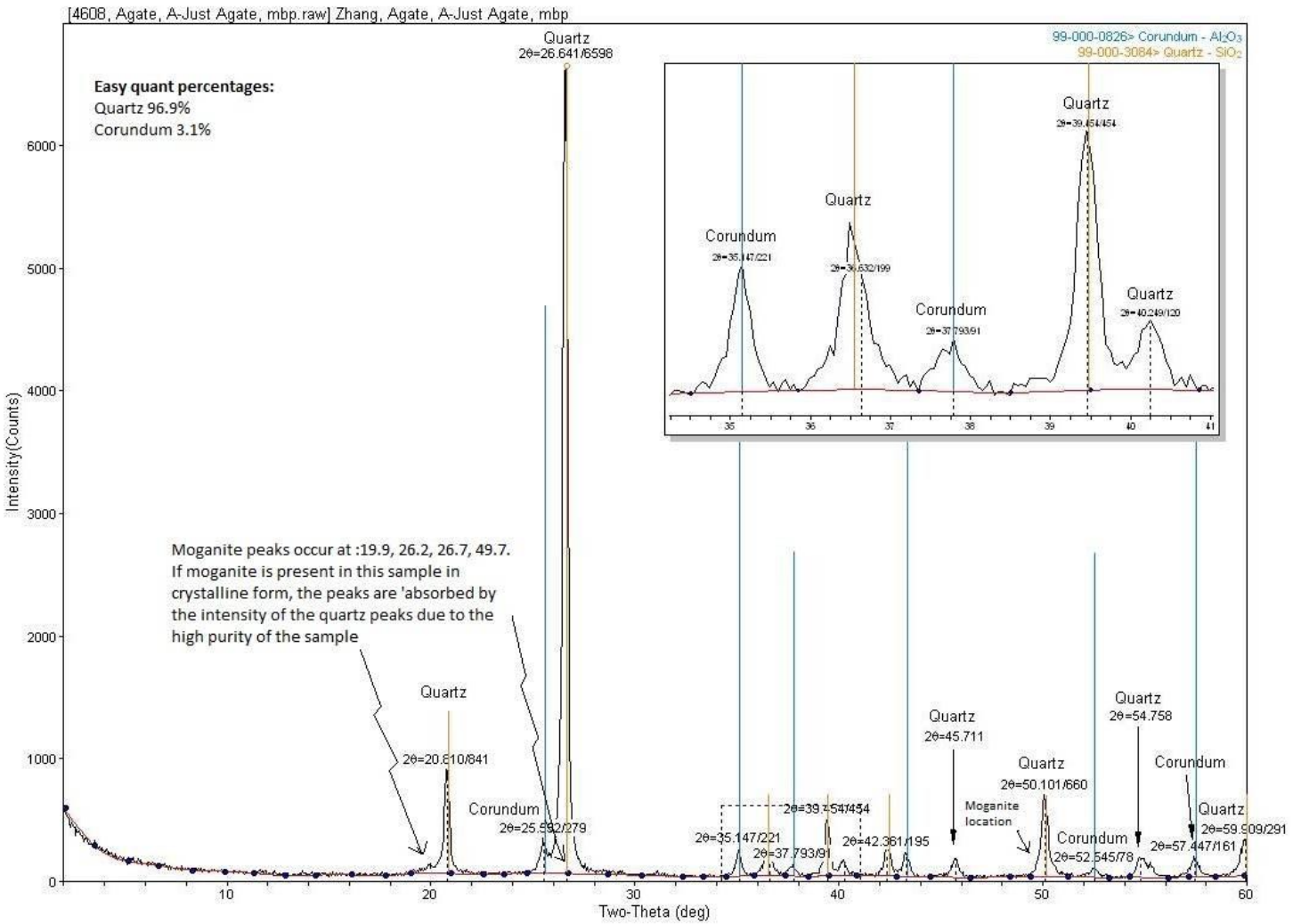

Figure 2.7 X-ray powder diffraction results. Because of the hardness of agate, we used corundum to powder the sample.

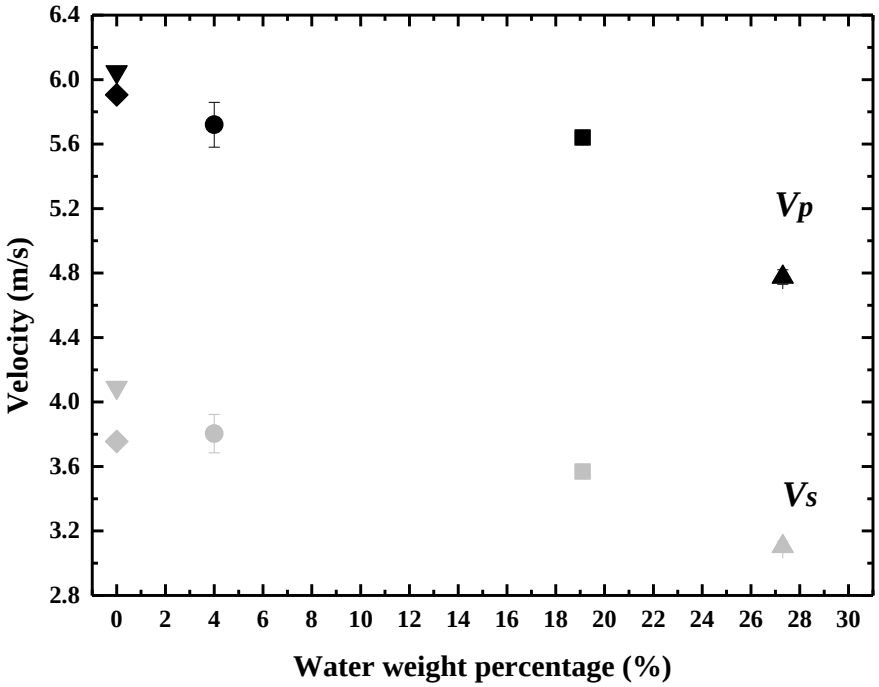

Figure 2.8 Water content and acoustic wave velocities of different silica samples. Black symbols: P-wave mode. Grey symbols: S-wave mode. Triangles: hyalite. Squares: wood opal. Circles: agate. Diamond: silica glass results from ultrasonic studies (Zhang et al, 2011). Upside-down triangles: quartz velocities using Viogt-Reuss-Hill averaging from single-crystal studies (Bass, 1995).

Chapter 3 MgO elastic properties measurements up to 19Gpa

Abstract

Grain boundaries constitute a substantial fraction of the volume in polycrystals and have the potential to significantly influence the physical and chemical properties, including elastic properties. The effective elastic behaviors of grain boundaries are still poorly understood. Here, acoustic aggregate compressional and shear wave velocities of polycrystalline MgO up to 19 GPa pressures were measured by Brillouin scattering at room temperature, from which their pressure derivatives were obtained. The signal-to-noise ratio and the sharpness of the Brillouin peaks increases with the decreasing grain size. Brillouin peaks are broad and roughly symmetric in shape. Peak shifts and velocities of the fine-grained MgO are close to the velocities obtained from single-crystal MgO measurements, and within 2% anisotropy. The grain boundaries do attribute to the elastic properties to some extent. The implications of our observations for the interpretation of Brillouin scattering results from polycrystalline materials are discussed.

3.1 Introduction

Polycrystalline samples of geologic materials and industrial ceramics have a variety of grain sizes, typically ranging from a few nanometers to tens of microns. By changing

only one parameter of a given synthesis technique, such as heating rate (Stanciu et al, 2001; Shen et al., 2002) and applied pressure (Munir et al., 2006) of spark plasma sintering, different grain size polycrystals may be obtained. However, the variations of elasticity, specifically sound velocities, due to the grain size effects are still poorly understood.

Polycrystalline minerals consist of a substantial volume fraction of the intercrystalline materials, mostly grain boundaries, which may significantly influence material elasticity, as well as other physical and chemical properties (Marquardt et al., 2011). A grain boundary is an interface between two crystals of the same structure (Bollmann, 1970; Thibault-Penisson and Preiester, 2011). An extensive body of previous work has been done on grain boundary plastic effects, including deformation mechanisms (Gemperlová et al, 2002, 2004); the role of grain boundaries in creep and in high temperature plasticity with an extension to superplasticity (Weertman, 1955, 1957; Fionova et al., 1993; Beaudoin and Tamtsia, 2004); the response of grain boundaries to fractures and fracture propagation, with particular focus on the effect of segregation on intergranualr brittleness (Chen et al., 1990; Faulkner, 1996; Hofmann, 1996; Vogt et al., 2007); the behavior of boundaries subjected to high- and low-temperature fatigue on polycrystals, with a few key elements (Saxena and Antolovich, 1975; Rémy et al., 1978; Xiao et al., 2006). However, the grain boundary effects resulting in material elasticity

remains large uncertainty.

In this paper we report Brillouin scattering measurements of the elastic wave velocities of fine-grained MgO polycrystalline material at high pressures up to 19 GPa.

3.2 Experimental details

3.2.1 Sample Preparation

Brillouin scattering experiments were performed on three different polycrystalline MgO samples (Table 3.1). Samples were prepared using spark plasma sintering (Guignard et al., 2011), resulting in dense fine-grained material that is sufficiently transparent to transmit the visible light used in Brillouin scattering. Samples were ground and polished into plate-like shapes (Figure 3.1) for symmetric geometry Brillouin scattering measurements at room conditions and also at high pressure using a diamond anvil cell (DAC). Water is normally used as a lubricant in grinding and polishing of samples. However, MgO readily reacts with water to form brucite, Therefore, we used mineral oil as a lubricant during the preparation of the MgO samples.

3.2.2 High-Pressure Experiments

The generation of the high pressure relies on a simple principle:

$$p = \frac{F}{A},$$

where p is the pressure, F the applied force, and A the area. Therefore high pressure can be achieved by applying a moderate force on a sample with a small area, rather than

applying a large force on a large area. To minimize deformation and failure of the anvils that apply the force, they must be made from an extremely hard and virtually incompressible material, such as diamond. Another requirement is that the anvil material must be transparent to visible light for spectroscopy. Therefore diamond is a promising candidate for an anvil material (Jayaraman, 1983, 1986).

Two types of DACs were used in the high-pressure measurements (Figure 3.2): 1) A 3-screw Merrill-Bassett style cells, with a 90 °conical opening (Merrill and Bassett, 1974; Jayaraman, 1983) and 2) A 4-screw piston-cylinder type diamond cells, with a 60 °conical opening (Mao and Hemley, 1996). Stainless steel gaskets were pre-indented to 50 ~ 60 μm thick and holes with diameters of 135 ~ 165 μm (nearly half size of the diamond culets, 250 ~ 300 μm) were machined using a micro electric discharge system to form sample chambers. Figure 3.3 shows the diamond anvil and the compressed gasket. Sodium chloride (NaCl) was used as pressure medium to simulate quasi-hydrostatic environment. Ruby fluorescence was applied to calculate the pressure using scale from Mao et al.(1986).

The DAC was used primarily in laboratories engaged in geological interest research where very high pressures simulating the earth's interior were desired, while the accuracy in the value of the pressure was not yet of primary importance. This situation changed dramatically when the high-pressure group at the National Bureau of Standards (NBS),

under the ever-present prodding of management, developed a better method for measuring pressures in the DAC (Piermarini and Block, 2001).

The main fluorescence lines (the R-line doublet lines) were intense and sharp, and the lines shifted toward the red end of the spectrum with increasing pressure (Figure 3.4; King and Prewitt, 1980; Chijioke et al. 2005). Relatively, ruby is chemically inert, and the fluorescence signal is pronounced. Hence, only a very small amount of ruby crystal could be enough to detect pressure in situ using without interfering with any other experimental specimen in the chamber (King and Prewitt, 1980; Piermarini and Block, 2001; Chijioke et al. 2005; Heiman, 2012). The wavelength of the R1 ruby fluorescence line corresponding to the pressure has become a widely used standard for measuring pressure in the DAC.

Several ruby spheres were placed around the MgO sample and experimental pressures were calculated from the ruby fluorescence R1 shift (Mao et al. 1978). Pressure was checked both before and after Brillouin measurements and the difference was within their mutual uncertainties. NaCl sound velocities were checked at each pressure point to compare with the ruby fluorescence results (Campbell and Heinz, 1992).

3.3 Results and discussions

Brillouin measurements were performed on MgO#1 (Table 3.1) at ambient temperature and pressure (1 atm). Several sample positions were probed to obtain a

representative sampling of the average peak positions. Only two data points were obtained for shear wave velocity (Table 3.2); other spectra did not show what we consider to be reasonable quality shear modes. The shear wave peaks of the spectra are broad and the signal-to-noise ratio is low (Figure 3.5).

Brillouin measurements were performed on MgO#2 (Table 3.1) at ambient temperature and two different pressure points, including the one at ambient pressure. At 1-atm, no convincing Brillouin spectrum is obtained due to the large amount of elastically scattered light from grain boundaries in the translucent sample. Brillouin scattering spectra were collected when the sample was both in the air and suspended in a refractive index liquid. The liquid was present to protect the sample from the reaction with atmospheric water, and to reduce the intensity of elastic scattering. The sample was placed within the sample chamber in a DAC and pressurized to 6.61 Gpa using NaCl as the pressure medium. Only a few data points were obtained, but the data quality is still poor (Table 3.2; Figure 3.5).

The quality of data from MgO#1 and MgO#2 were inferior to the spectra obtained with Mg15 (see below). Therefore, we use only the data from Mg15 in this study, and data from samples #1 and #2 are not considered further.

Brillouin measurements were performed on Mg15 (Table 3.1) at ambient temperature and seven different pressure points (including ambient pressure) (Table 3.3). At each

pressure point, Brillouin spectra were collected over an angular range of 180 ºspaced 30 º apart in the sample plane, except for the 1 atm data. At room pressure, Brillouin spectra were collected 15 ºapart instead of 30 º. The Brillouin peaks were generally of very good quality with a high signal-to-noise ratio and clearly separated peaks, except for a few cases where the compressional velocity of the NaCl pressure-transmitting medium overlapped with the shear peaks of the sample (Figure 3.6). To differentiate the peaks for NaCl and MgO, Brillouin spectra were collected on areas of the sample chamber that contained both MgO+NaCl and also NaCl only (Whitfield et al., 1976; Campbell and Heinz, 1992; Sinogeikin et al, 2006). To obtain high quality spectra, long collection times (more than one hour) were necessary for the high pressure experiments, whereas shorter collection time (about 30 minutes) for 1 atm measurements.

From sample MgO#1, MgO#2 and Mg15, the signal-to-noise ratio and the sharpness of the Brillouin peaks increase with the decreasing grain size, average 7μm, less than 5μm, less than 1μm respectively. Brillouin spectra from Mg15 sample show broad peaks that are roughly symmetric in shape. Peak shifts and velocities of the fine-grained MgO are comparable to the velocities obtained from single-crystal MgO measurements using Voigt-Reuss-Hill averaging (Hill, 1952; Sinogeikin and Bass, 1999). The results on Mg15 indicate that the anisotropy of the polycrystalline MgO velocities is within 2% (Table 3.4), which also indicates that there is no preferred orientation for the MgO polycrystals.

Comparing the width of Brillouin peaks at different pressures, we figured out that the sharpness of the peaks increases as the increasing pressure (eg. Figure 3.6), which is consistent with the change of MgO anisotropy (Sinogeikin and Bass, 2000). Grain boundaries may also attribute to the sharpness change. The grain boundaries become more difficult to observe as the increasing pressure (Figure 3.7). This phenomenon is due to two resaons: A) we are pressurizing sintering the MgO while increasing the pressure in DAC; B) the refractive index contrast between the sample and the pressure medium becomes smaller as the increasing pressure.

Previous studies on non-hydrostatic loading experiments indicate that polycrystalline MgO has a profound acoustic wave velocities drop, about 30% to 50% drop, compared to the single-crystal studies (Marquardt et al., 2011; Gleason et al., 2011). In contrast, our work shows a difference within 10% (Figure 3.8). Previous studies on single-crystal MgO suggest that MgO is highly anisotropic elastically with values of $\Delta Vp/Vp^{*}$ = 10.6%, $\Delta Vs/Vs^{*}$ = 20.8%, where ΔVp and ΔVs are the differences between the maximum and minimum velocities for the crystal longitudinal and shear, respectively; and Vp^{*} and Vs^{*} are aggregate velocities calculated using the Hill averaging scheme (Hill, 1952; Sinogeikin and Bass, 2000). Our results include several data points even fall within the anisotropy bounds for single-crystal MgO (Figure 3.9), which is also comparable to the hydrostatic studies (Schreiber et al., 1973; Spetzler, 1988; Sinogeikin and Bass, 2000)

and quasi-hydrostatic study (Murakami et al, 2009). Hence, we cannot draw a conclusion that the influence of the grain boundaries is the major reason for the velocity drop.

Marquardt et al. (2011) and Gleason et al. (2011) used a non-hydrostatic loading, directly loading sintered MgO without pressure medium in the sample chamber,-for their high pressure work. In our experiments, NaCl was used as a pressure medium, because it is a relatively soft solid which produces a quasi-hydrostatic environment. Nonhydrostaticity caused by use of solid pressure medium in high-pressure Brillouin spectroscopy is a major source of error in determination of the pressure derivatives of the acoustic wave velocities (Sinogeikin and Bass, 2000; Zhang et al.,2012); we therefore interpret the pronounced velocities drop as a result of the nonhydrostaticiy, and the elasticity of polycrystalline MgO behaves similarly to single-crystal MgO.

3.4 Conclusions

Brillouin scattering experiments on fine-grained MgO demonstrate that grain size contributes to the effective elastic properties of polycrystalline materials, specifically acoustic velocities. The width of the Brillouin peaks and the uncertainty of Brillouin peaks decrease with the decreasing grain size, from average 7μm, to less than 5μm to less than 1μm respectively.

The polycrystalline MgO has a lower longitudinal velocity and shear velocity than the single crystal, but are almost consistent with the single crystal data. Grain boundaries

influence the effective elastic behaviors of polycrystalline materials, but it is not the major reason for the profound velocity drop. Nonhydrostatic stress in the sample chamber of a diamond cell is the major source of error in determination of the pressure derivatives of the acoustic wave velocity.

Reference

Bass, J.D. (2007) Theory and Practice – Techniques for Measuring High P/T Elasticity. *Treatise on Geophysics*, 2, 269-291.

Beaudoin, J.J. and Tamtsia, B.T. (2004) Creep of Hardened Cement Paste - The Role of Interfacial Phenomena. *Interface Science*, 12(4), 356-360.

Bollmann, W. (1970) *Crystal Defects and Crystalline Interfaces*, Springer-Verlag, Berlin.

Campbell, A.J. and Heinz, D.L. (1992) A High-Pressure Test of Birch's Law. *Science*, 257, 66-68.

Chen, S.P., Voter, A.F., Albers, R.C., Boring, A.M. and Hay, P.J. (1990). Investigation of the effects of boron on Ni3Al grain boundaries by atomistic simulations. *Journal of Materials Research*, 5, 955-970.

Chijioke, A.D., Nellis, W. J., Soldatov, A. and Silverab, I.F. (2005) The ruby pressure standard to 150 GPa. *Journal of Applied Physics*, 98, 114905

Davies, G.F. and Dziewonski, A.M. (1975) Homogeneity and constitution of the Earth's lower mantle and outer core. *Physics of the Earth and Planetary Interiors*, 10, 336-343.

Faulkner, R. G. (1996) Segregation to boundaries and interfaces in solids. *International Materials Reviews*, 41(5), 198-208.

Fionova, L., Konokenko, O., Matveev, V., Priester, L., Lartigue, S. and Dupau, F. (1993) Heterogeneities of grain boundary arrangement in polycrystals. *Interface Science*, 1(3), 207-211.

Gemperlová, J., Jacques, A., Gemperlea, A., Vystavela, T., Zárubováa, N., and Janecekc, M. (2002) In-Situ Transmission Electron Microscopy Observation of Slip Propagation in Σ3 Bicrystals. *Materials Science and Engineering: A*, 324(1-2), 183-189.

Gemperlová, J., Polcarová, M., Gemperle, A. and Zárubová, N. (2004) Slip Transfer Across Grain Boundaries in Fe–Si Bicrystals. *Journal of Alloys and Compounds*, 378(1–2), 97-101.

Gleason, A. E., Marquardt, H., Chen, B., Spezial, S., Wu, J. and Jeanloz, R. (2011) Anomalous sound velocities in polycrystalline MgO under non-hydrostatic compression. *Geophyical Research Letters*, 38.

Guignard, J., Bystricky, M. and Bejina, F. (2011) Dense fine-grained aggregates prepared by spark plasma sintering (SPS), an original technique in experimental petrology. *European Journal of Mineralogy*, 23(3):323-331

Heiman, D. (2012) Spectroscopy of Ruby Fluorescence. http://nuweb.neu.edu/dheiman/3600/RUBY.pdf

Hill, R. (1952) The elastic behavior of a crystalline aggregates. *Proceedings of the Physical Society Section A*, 65, 349–354.

Hofmann, S. and Leiĉek, P. (1996) Solute segregation at grain boundaries. *Interface Science*, 3(4), 241-267.

Jayaraman, A. (1983). Diamond Anvil Cell and High-Pressure Physical Investigations. *Reviews of Modern Physics*, 55, 65–108.

Jayaraman, A. (1986). Ultrahigh pressures. *Review of Scientific Instruments*, 57, 1013-1031.

Karki, B.B., Wentzcovitch, R.M., de Gironcoli, S. and Baroni, S. (1999) First-Principles Determination of Elastic Anisotropy and Wave Velocities of MgO at Lower Mantle Conditions. *Science*, 26, 1705-1707.

King, H.E. and Prewitt, C.T. (1980) Improved pressure calibration system using the ruby R1 fluorescence. *Review of Scientific Instruments*, 51, 1037-1039

Mao, H. K. and Bell, P.M. (1978) Design and varieties of the megabar cell, in *Carnegie Institution of Washington Year Book*, 77, 904-908.

Mao, H.K., Bell, P.M., Shaner, J.W. and Steinberg, D.J. (1978) Specific volume measurements of Cu, Mo, Pd, and Ag and calibration of ruby R1 fluorescence pressure gauge from 0.06 to 1 Mbar. *Journal of Applied Physics*, 49(6), 3276-3283.

Mao, H.K., Xu, J., and Bell, P.M. (1986) Calibration of the ruby pressure gauge to 800 kbar under quasi-hydrostatic conditions. *Journal of Geophysical Research*, 91, 4673–4676.

Marquardt, H., Gleason, A.E., Marquardt, K., Speziale, S., Miyagi, L., Neusser, G., Wenk, H.-R. and Jeanloz, R. (2011) Elastic properties of MgO nanocrystals and grain boundaries at high pressures by Brillouin scattering. *Physical Review B*, 84, 0641311-0641319

Merrill, L., and Bassett, W.A. (1974) Miniature diamond anvil pressure cell for single-crystal X-ray diffraction studies. *Review of Scientific Instruments*, 45(2), 290-294.

Munir, Z.A., Anselmi-Tamburini, U. and Ohyanagi, M. (2006). The effect of electric field and pressure on the synthesis and consolidation of materials: A review of the spark plasma sintering method. *Journal of Materials Science*, 41(3), 763-777.

Murakami, M., Ohishi, Y., Hirao, N., & Hirose, K. (2009). Elasticity of MgO to 130 GPa: Implications for lower mantle mineralogy. *Earth and Planetary Science Letters*, 277(1), 123-129.

Piermarini, G. and Block, S. (2001) The Diamond Anvil Pressure Cell. *A Century of Excellence in Measurements, Standards, and Technology: A Chronicle of Selected NBS/NIST Publications 1901-2000*, NIST Special Publication 958, 100-103

Rémy, L., A. Pineau, and B. Thomas. (1978) Temperature Dependence of Stacking Fault Energy in Close-Packed Metals and Alloys. *Materials Science and Engineering*, 36(1), 47-63.

Saxena, A. and Antolovich, S.D. (1975) Low cycle fatigue, fatigue crack propagation and substructures in a series of polycrystalline Cu-Al alloys. *Metallurgical Transactions A*, 6(9), 1809-1828.

Schreiber, E., Anderson, O.L. and Soga, N. (1973) *Elastic Constants and Their Measurements*, pp. 25-31, McGraw‐Hill, New York.

Shen, Z., Johnsson, M., Zhao, Z. and Nygren, M. (2002), Spark Plasma Sintering of Alumina. *Journal of the American Ceramic Society*, 85: 1921–1927.

Sinogeikin, S.V. and Bass, J. D. (1999) Single-crystal elasticity of MgO at high pressure. *Physical Review B*, 59, 14141–14144.

Sinogeikin, S.V. and Bass, J.D. (2000) Single-Crystal Elasticity of Pyrope and MgO to 20 GPa by Brillouin Scattering in the Diamond Cell. *Physics of the Earth and Planetary Interiors*, 120(1–2), 43-62.

Sinogeikin, S.V., Bass, J.D., Prakapenka, V., Lakshtanov, D., Shen, G., Sanchez-Valle, C. and Rivers, M. (2006) Brillouin spectrometer interfaced with synchrotron radiation for simultaneous x-ray density and acoustic velocity measurements. *Review of Scientific Instruments*, 77(10), 1039501-1039511.

Spetzler, H. (1988), Equation of state of polycrystalline and single-crystal MgO to 8 kilobars and 800 °K, in *Elastic Properties and Equations of State*, edited by T. J. Shankland and J. D. Bass, pp. 290–304, AGU, Washington, D. C.

Stanciu, L.A., Kodash, V.Y. and Groza, J.R. (2001). Effects of heating rate on densification and grain growth during field-assisted sintering of α-Al2O3 and MoSi2 powders. *Metallurgical and Materials Transactions A*, 32(10), 2633-2638.

Thibault-Penisson, J. and Preiester, L. (2011) Grain boundary structures and defects, in *Grain boundaries and crystalline plasticity*; ISTE Ltd, UK, and John Wiley & sons, Inc, NJ.

Xiao, L., Chen, D.L. and Chaturvedi, M.C. (2006) Effect of Boron on Fatigue Crack Growth Behavior in Superalloy IN 718 at RT and 650 ℃. *Materials Science and Engineering: A* 428(1–2), 1-11.

Vogt, J., Verleene, A., Serre, I., Balbaud-Célérier, F., Martinelli, L. and Terlain, A. (2007) Understanding the Liquid Metal Assisted Damage Sources in the T91 Martensitic Steel for Safer use of ADS. *Engineering Failure Analysis*, 14(6), 1185-1193.

Weertman, J. (1955) Theory of Steady‐State Creep Based on Dislocation Climb. *Journal of Applied Physics*, 26, 1213-1217.

Weertman, J. (1957) Steady‐State Creep through Dislocation Climb. *Journal of Applied Physics*, 28, 362-364.

Whitfield, C.H., Brody, E.M. and Bassett, W.A. (1976) Elastic moduli of NaCl by Brillouin scattering at high pressure in a diamond anvil cell. *Review of Scientific Instruments* 47, 942-947.

Zhang, J.S., Dera, P. and Bass, J.D. (2012). A new high-pressure phase transition in natural Fe-bearing orthoenstatite. *American Mineralogist*, 97(7), 1070-1074.

Tables

Table 3.1 MgO Sample descriptions

	MgO#1	MgO#2	Mg15
Grain Size (μm)	~5 to 10	~5	<1
Sample Dimension (μm^2)	~100×300	~150×300	~200×400
Thickness after preparation (μm)	~15	~20	~50 (ambient pressure) ~35 (high pressure)
Transparency after preparation	Translucent	Translucent	Transparent

1. Grain size for MgO#1 and MgO#2, and sample thickness are estimated using optical microscopy.
2. Mg15 was prepared from a commercial nano MgO powder - grain size about 50 nm. It was sintered using SPS (run number AK272) at 750℃ and 100 MPa for 10 minutes. Temperature was controlled by a thermocouple. The ramp up in temperature lasted 7 minutes, dwell was 10 minutes and ramp down was 20 minutes. Pressure was increased when target temperature was reached.

Table 3.2 Sample MgO#1 and MgO#2 Results of Brillouin spectral data

	MgO#1		MgO#2	
Chi angle	360_1	360_2	360	310
Vs (m/s)	4488	4718		6076
Vp (m/s)			9839	9989

1. MgO#1: experiments were performed at 1-atm.
   MgO#2: experiments were performed under 6.61Gpa.

Table 3.3 Sample Mg15 Results of Brillouin spectral data

1 atm measurements												
Chi Angle	362	330	315	300	285	270	255	240	225	210	195	180
Vs (m/s)	5572	5588	5575	5636	5628	5616	5673	5592	5661	5656	5634	5540
Vp (m/s)	9119						9611				9136	9422

P (Gpa)	19.39(5)		13.24(10)		8.64(1)		5.63(5)		2.49(4)	0.28(3)
Chi angle	Vs (m/s)	Vp (m/s)	Vs (m/s)	Vp (m/s)	Vs (m/s)	Vp (m/s)	Vs (m/s)	Vp (m/s)	Vp (m/s)	Vp (m/s)
360	6264	10226	6272	10376	5977	9836	5864	9693	9461	
330	6241	10262	6252	10276			5904	9635	9441	9216
300	6335	10475	6253	10325	5916	9694	5957	9726	9434	9250
270	6310	10422	6213	10278	5949	9743	5781	9537	9298	9170
240	6241	10380	6202	10304	5922	9706	5811	9516	9260	9334
210	6270	10316	6362	10560	5874	9672	5874	9641	9236	8843
180	6206	10175	6122	9987			5861	9692		9043

1. For 1 atm measurements, we used 362 °chi angle instead of 360.
2. For P = 0.28 Gpa, P = 2.49 Gpa, we only got the P-wave peaks in the spectra.
3. For those chi angles without velocities in the table, we did not get pronounced peaks at the specific pressure and chi angle.

Table 3.4 Sample Mg15 Brillouin spectra analysis

Pressure	Vs (m/s)	±σ	Vp (m/s)	±σ
1 atm	5614 ± 41	0.73%	9322 ± 237	2.54%
0.28 Gpa			9143 ± 175	1.91%
2.49 Gpa			9355 ± 101	1.08%
5.63 Gpa	5865 ± 58	0.99%	9634 ± 80	0.83%
8.64 Gpa	5928 ± 39	0.66%	9730 ± 64	0.66%
13.24 Gpa	6239 ± 73	1.17%	10301 ± 170	1.65%
19.39 Gpa	6267 ± 44	0.70%	10322 ± 107	1.04%

1. ±σ: Standard deviation of peak positions
2. For single crystal, Voigt-Reuss-Hill averaging velocities at room condition, Vp: 9687m/s, Vs: 6033m/s (Sinogeikin and Bass, 1999).

Table 3.5 Aggregate elastic moduli of MgO (Mg15) as a function of Pressure

P (Gpa)	ρ (g/cm^3)	G (Gpa)	K (Gpa)
0.0001	3.584(1)	112.97(10)	160.83(10)
0.28(3)	3.590(3)	113.07(10)	149.33(10)
2.49(4)	3.637(4)	119.30(10)	159.27(10)
5.63(5)	3.702(6)	127.32(10)	173.84(10)
8.64(1)	3.761(1)	132.13(10)	179.86(10)
13.24(10)	3.846(5)	149.71(20)	208.43(20)
19.39(5)	3.952(6)	155.20(10)	214.14(10)

Figures

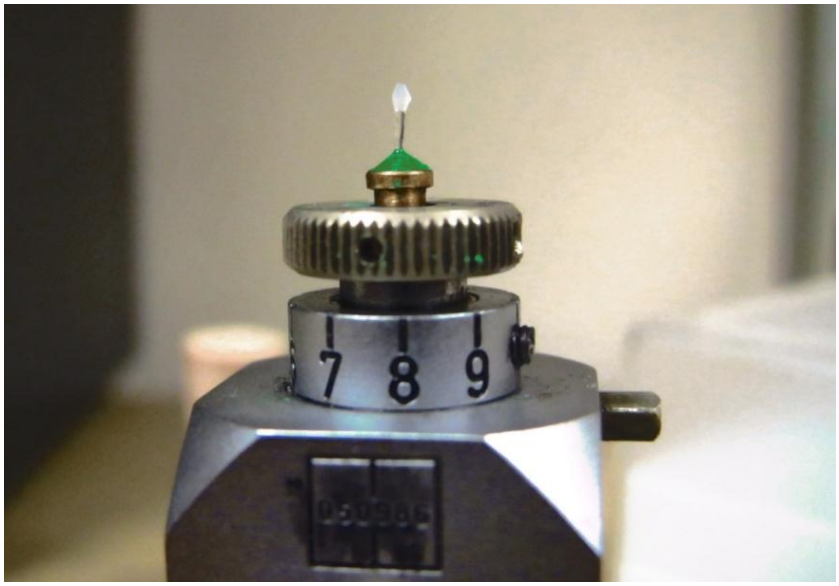

Figure 3.1 Photograph of prepared Mg15 sample mounting on the goniometer ready for the ambient condition measurements. The dimension is around 300μm×200μm×80μm.

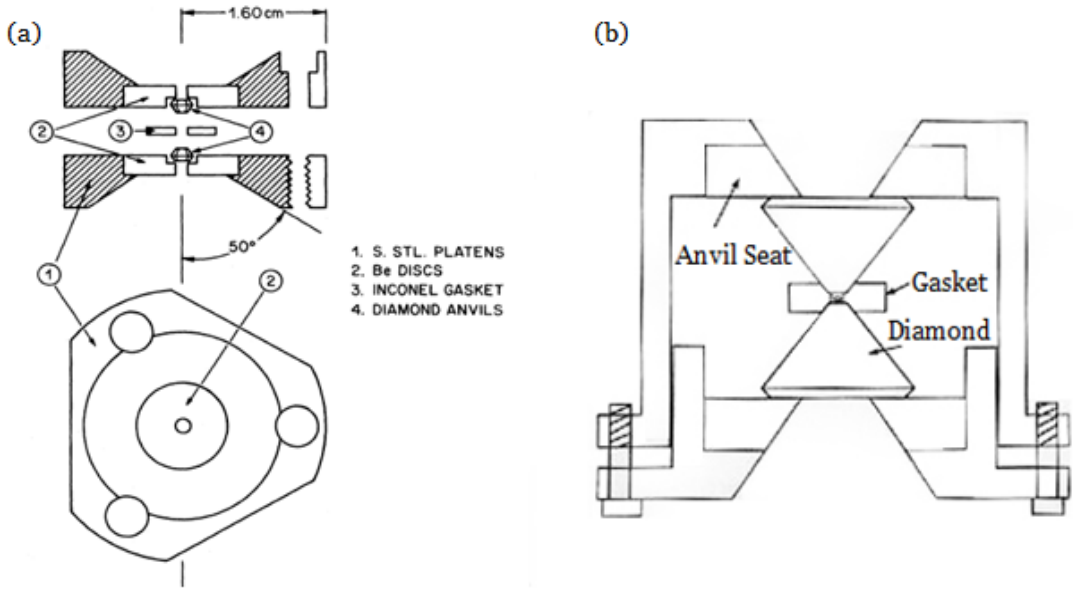

Figure 3.2 (a) Schematic of a Merrill-Bassett miniature cell. The diamonds are set in Be backing plates and the thrust applied by tightening the three symmetrically located screws. (Jayaraman, 1983) (b) Schematic of a piston-cylinder diamond anvil cell. (Bass, 2007)

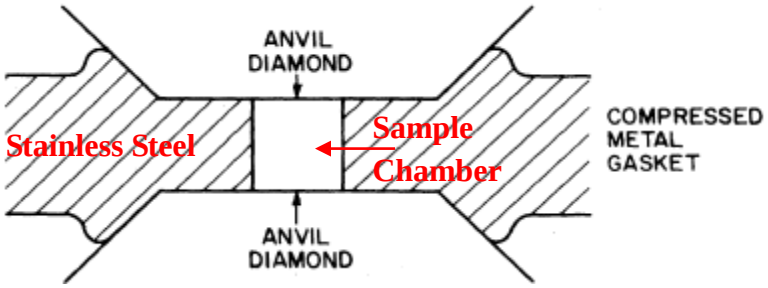

Figure 3.3 A schematic scratch of sample chamber and the compressed gasket between two anvil diamonds supported by the diamond culet edges (After Jayaraman, 1983).

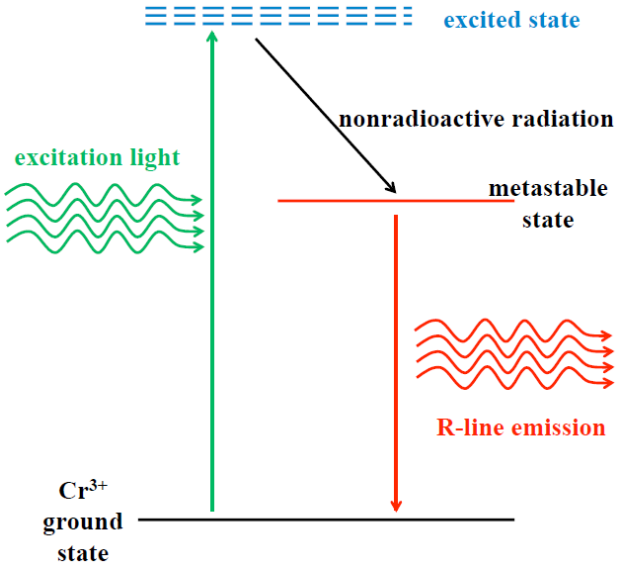

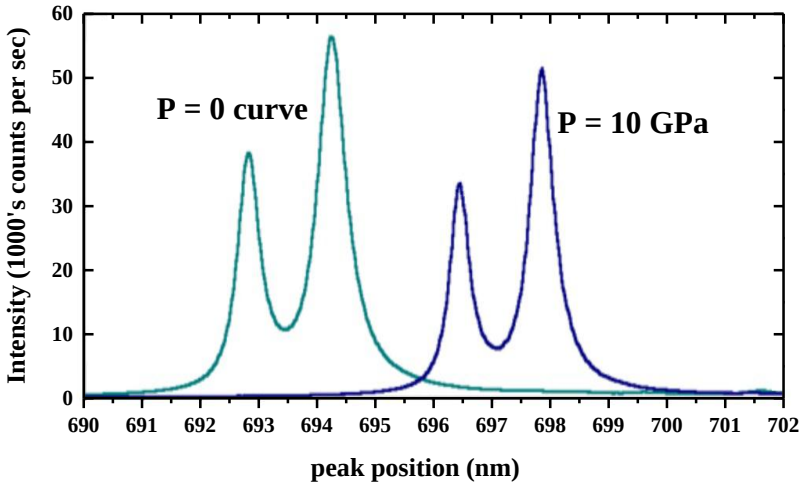

Figure 3.4 A schematic illustration of R-line emission (top) and an example of ruby fluorescence spectra (bottom). Cr ion substitutes for Al ion in Ruby. The right peak of the spectra is R1 peak.
(Can be retrieved http://geoweb.princeton.edu/research/MineralPhy/labtour/Ruby.html)

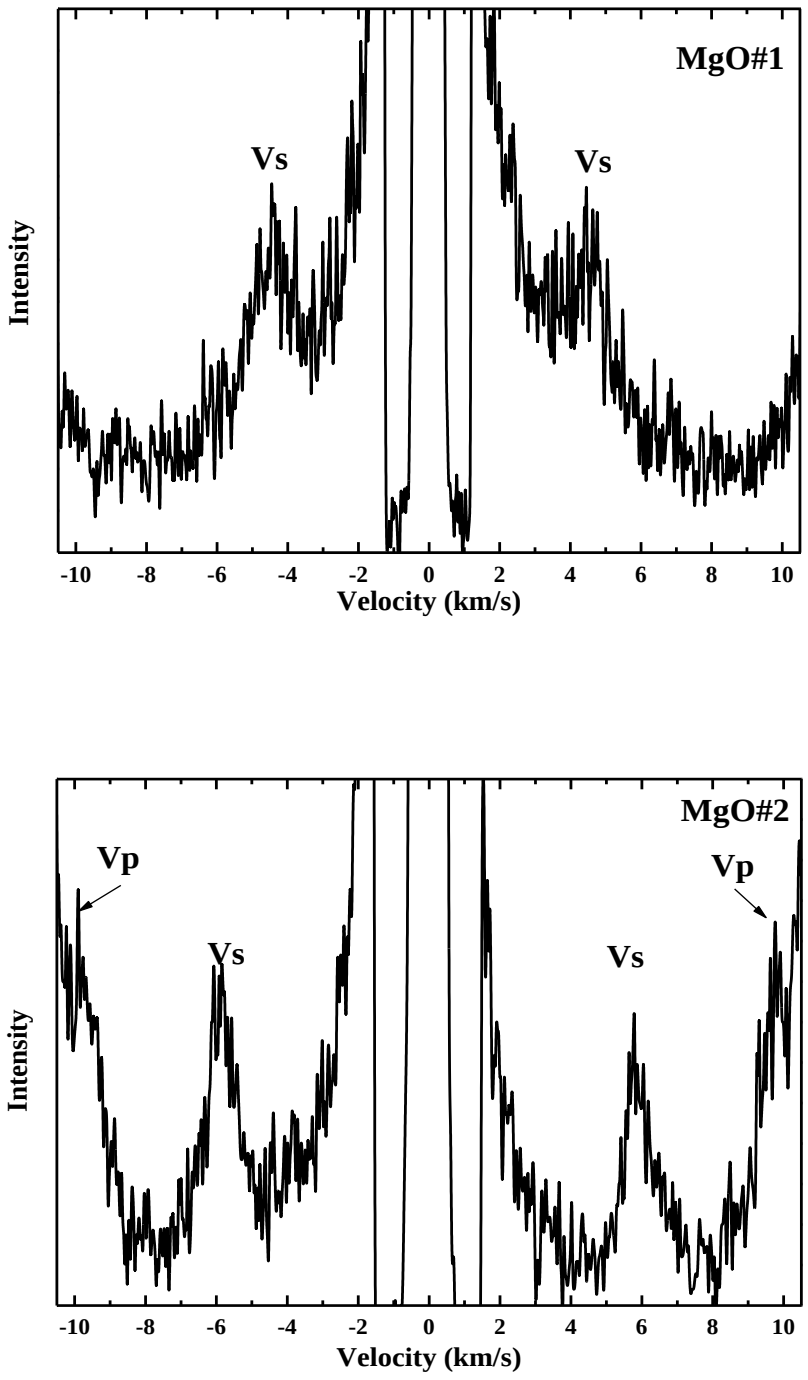

Figure 3.5 Two typical Brillouin spectra for MgO#1 and MgO#2 under different pressure conditions. Brillouin peaks are broad and roughly symmetric with a low signal-to-noise ratio.

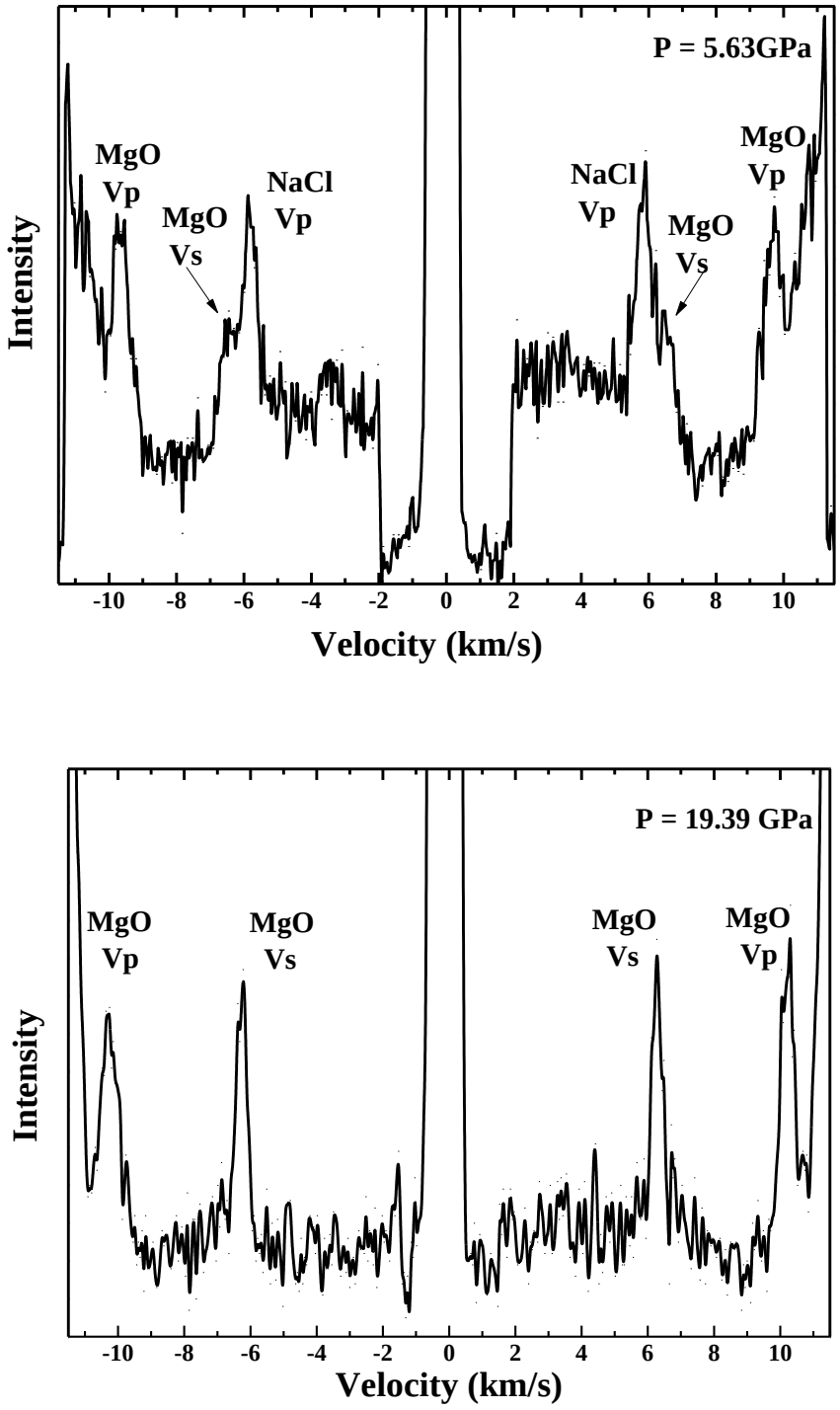

Figure 3.6 Two typical Brillouin spectra for Mg15 under different pressure conditions. As pressure increases, the velocities' peaks for MgO become sharper and faster; the velocities' peaks for NaCl becomes weaker due to the thinner layer.

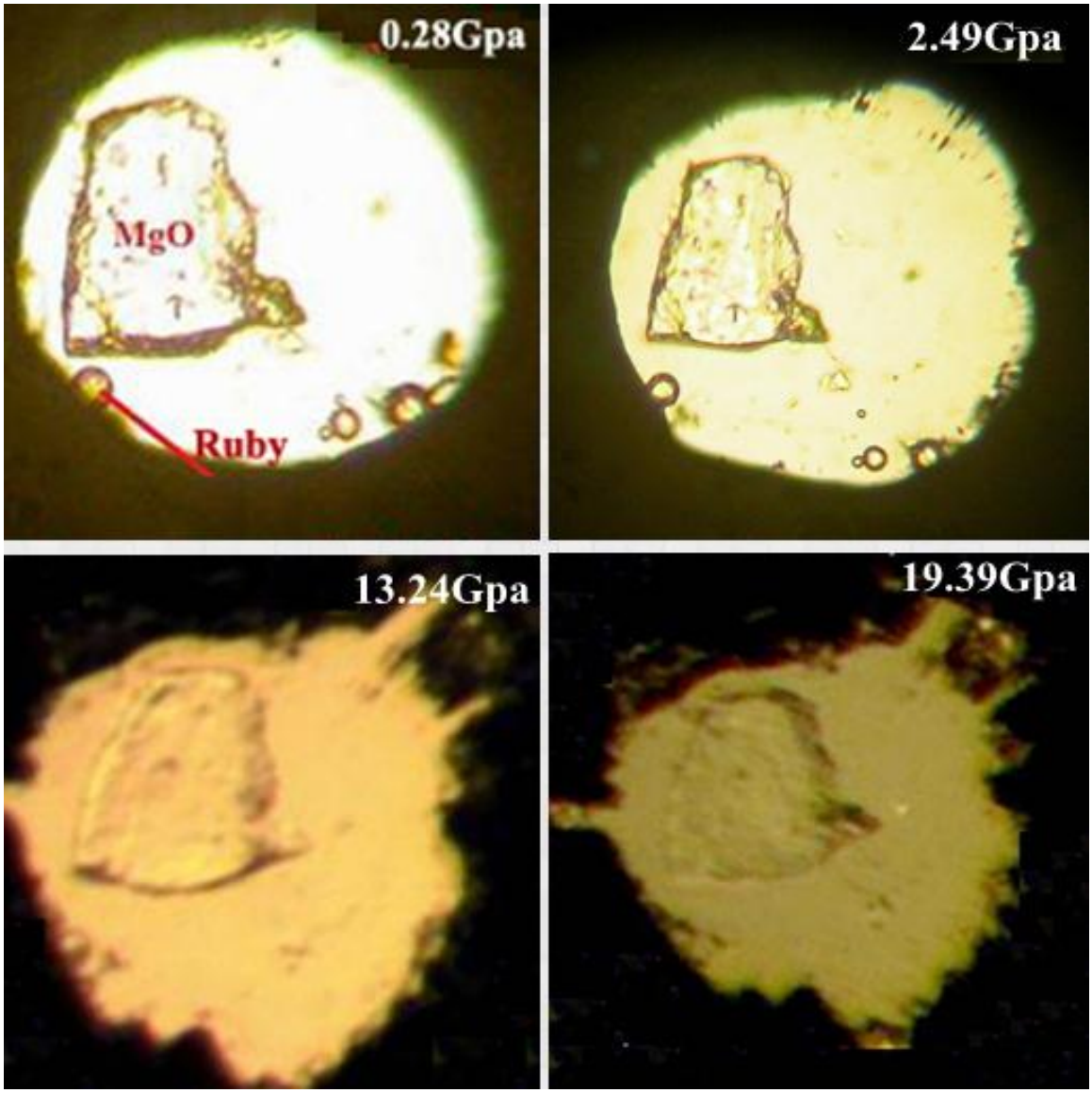

Figure 3.7 Photographs of sample chamber at different pressure points. The gasket hole deformed as the increasing pressure. The smoothness of the samples surface increases with the increasing pressure.

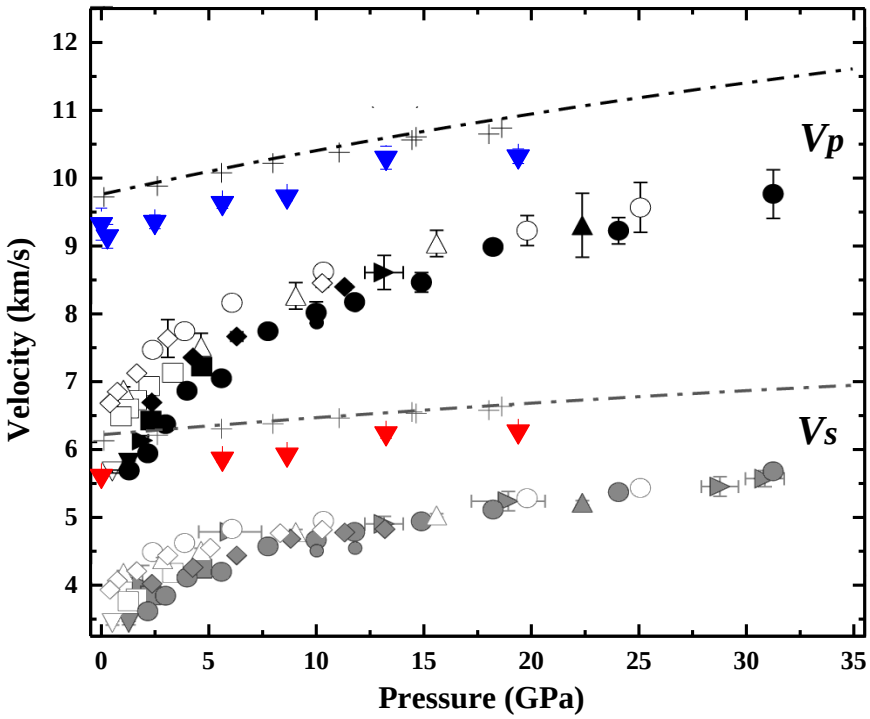

Figure 3.8 Pressure dependence of compressional and shear velocities of polycrystalline MgO. Colored solid upside down triangles: this study, blue and red represent compressional and shear mode, respectively. Crosses: Voigt–Reuss–Hill average velocities from single-crystal experiments assuming a random orientation distribution (dark grey: compressional mode; light grey: shear mode; Sinogeikin and Bass, 2000). Dash-dotted curves: computational results (Karki et al., 1999). Filled and open grey circles and diamonds: data collected in compression and decompression non-hydrostatic studies of nc-MgO powder, respectively (Marquardt et al., 2011). Circles: velocities measured in reflection geometry. Diamonds: data set measured with NaCl as pressure-transmitting medium. Filled and open grey triangles and squares: non-hydrostatically loaded polycrystals studies by Gleason et al, 2011. Squares: 5-10 mm pressed powder. Triangles: 1 mm pressed powder. (After Marquardt et al., 2011)

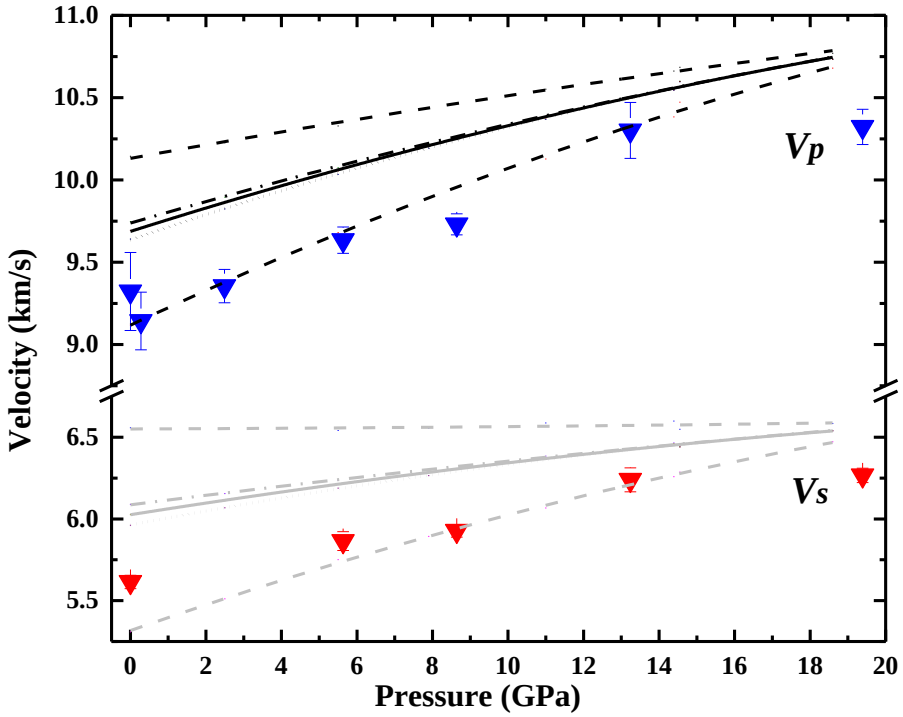

Figure 3.9 Pressure dependence of compressional and shear velocities of polycrystalline MgO comparing to the single-crystal work. This study: blue and red triangles (compressional and shear, respectively). Previous single-crystal work: black and grey lines (compressional and shear, respectively; Sinogeikin and Bass, 2000). Dash lines: absolute maximum and minimum velocities from single-crystal experiments. Dash dot lines: Voigt bound from single-crystal experiments. Dot lines: Reuss bound from single-crystal experiments. Solid lines: Voigt–Reuss–Hill average velocities from single-crystal experiments assuming a random orientation distribution.

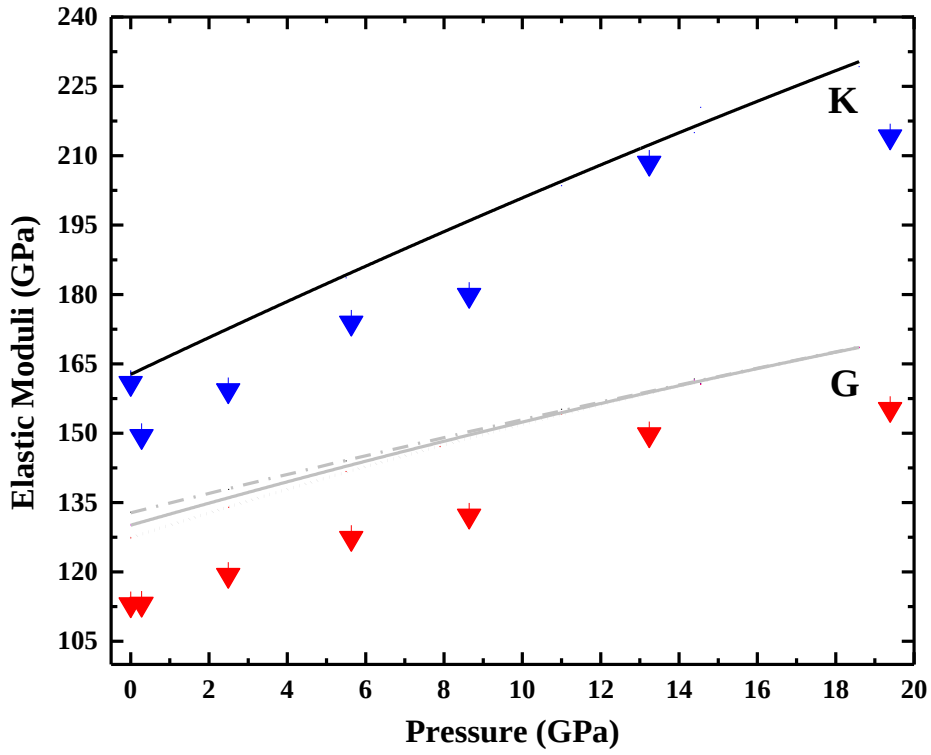

Figure 3.10 Pressure dependence of aggregate elastic modulus in MgO. This study: blue and red triangles. At pressure points 0.28Gpa and 2.49Gpa, we estimated the shear wave velocities using second-order fit. Previous single-crystal work: black and grey lines (Sinogeikin and Bass, 2000). Dash dot lines: Voigt bound from single-crystal experiments. Dot lines: Reuss bound from single-crystal experiments. Solid lines: Voigt-Reuss-Hill average modulus from single-crystal experiments assuming a random orientation distribution. Voigt bond, Reuss bond and Voigt-Reuss-Hill average of bulk modulus are the same solid black line in this figure.